Biological and particulate contaminants in interfaces

by

Jia Su

Submitted to the Department of Civil & Environmental Engineering
in partial fulfillment of the requirements for the degree of

Master of Science in Civil & Environmental Engineering

at the

MASSACHUSETTS INSTITUTE OF TECHNOLOGY

February 2018

© Massachusetts Institute of Technology 2018. All rights reserved.

Signature redacted

Author ....
Department of Civil & Environmental Engineering
January 19, 2018

Certified by..... Signature redacted ....
Prof. Lydia Bourouiba
Assistant Professor
Thesis Supervisor

Signature redacted

Accepted by ....
Prof. Jesse Kroll
Chairman, Department Committee on Graduate Theses

ARCHIVES
MASSACHUSETTS INSTITUTE OF TECHNOLOGY
APR 18 2018
LIBRARIES

Biological and particulate contaminants in interfaces

by

Jia Su

Submitted to the Department of Civil & Environmental Engineering
on January 19, 2018, in partial fulfillment of the
requirements for the degree of
Master of Science in Civil & Environmental Engineering

Abstract

The transport of biological, chemical, or particulate contaminants shapes disease transmission, chemical spills, climate, ecology, and bio-hazard risks. Yet, little is understood on the mechanisms controlling droplet formation and selection of droplet sizes and contamination levels from a contaminated water bulk. Bubbles play a critical role in shaping this transfer of chemicals, particulates, and biological organisms from water to air. They surface, and eventually burst, emitting myriads of droplets into the air. Despite recent progress in our understanding of bubble formation and bursting at the air-water interface, the factors selecting the loads that they carry and emit into the air remain unknown in part due to limitation in direct measurements. In this thesis, we discuss a method of direct visualization and quantification of particulates contained in contaminated bubble films at interfaces. The calibration of this method is key to progress in our understanding of particulate transport from water to air. In particular, although our method allows to reveal contaminants within films via the appearance of spots, the exact link between the size of such spots and the size of the original particles or organisms, their shape, wetting, and the size of the film remain unexplored. In this thesis, we performed a series of systematic measurements and calibrations using bacteria, particles, and rods of various sizes and wetting properties to calibrate the spot sizes observed on contaminated bubbles and films. We rationalized the dependencies observed using a combination of optical ray-tracing and modelling of film distortion in the presence of contaminant. Our results have important implications for in situ study of particles and bacterial communities within large scale complex interfaces.

Thesis Supervisor: Prof. L. Bourouiba
Title: Assistant Professor

Acknowledgments

I would first like to express my sincere gratitude to my advisor Prof. Lydia Bourouiba, Esther and Harold E. Edgerton Career Development Assistant Professor of Civil and Environmental Engineering and Mechanical Engineering at the Massachusetts Institute of Technology, a talented teacher and passionate scientist, for the continuous support of my studies and research, for her patience, motivation, enthusiasm, and inspiration. She is one of the most brilliant, dedicated and determined women scientists I have ever met. Her guidance helped me throughout my research, study, and writing of this thesis. I could not have imagined having a better advisor and mentor.

I am extremely thankful to my labmate Stephane Poulain for his kind help throughout my research. He is not only my labmate but also my role model. He shared his excellent advice with me, helping to improve my skills in both coding and writing. I cannot express enough how thankful I am to him.

Besides, I would like to thank all the people who helped me with my research at MIT: Prof. Jesse H. Kroll for the moral support of all the graduate students in our department, Prof. Otto Cordero and his student Elise Ledieu for training us with bacterial culture skills, Prof. Benedetto Marelli and his student Yunteng Cao for their collabration, and Prof. Benjamin Kocar and his student Michael Chen for helping us with storage of our fragile bacteria.

My sincere thanks also goes to all my other labmates in the Fluid Dynamics of Disease Transmission Laboratory: Dr. Timothee Jamin, Dr. Youngsoo Joung, Yongji Wang, Maxime Inizan, Nicole Bustos, Vira Dhaliwal, Raj Dandekar, Skungkwon Lee, Nicholas Kwok, Baptiste Lafoux, and Max Louyot. Thanks for all the fun and support. Graduate school can be a difficult draining experience, but I am proud to say my experience here was intellectually exciting and fun.

Last but not the least, I would like to thank my parents Mrs. Yun Yun and Mr. Zhongjin Su for supporting me spiritually throughout my studies and entire life.

We gratefully acknowledge support of the MIT-Lincoln Laboratory through the ACC 645, of the NSF through CBET-1546990 and the MIT and Reed Funds.

Contents

1 Chemical, particle, and pathogen transfers **15**

1.1 Bubbles and contaminants 18

1.2 Water-air exchanges via bubbles 20

1.2.1 Physiology of a bubble 21

1.3 Overview of the project 22

2 Bubbles and contamination **25**

2.1 Bubbles in contaminated water 25

2.2 Bubbles and pathogens 26

2.3 Summary 29

3 Biological background **31**

3.1 Bacteria protocol 31

3.1.1 *Echerichia coli* 31

3.2 Methodology 32

3.2.1 Bacterial Culture 32

3.2.2 Protocols to make LB agar 33

3.2.3 *E.coli* culture from -80 °C freezers 35

3.2.4 Purification 36

3.3 Behavior of the bacteria liquid 37

3.3.1 OD and pH evolution 37

3.3.2 Surface tension 40

4 Schlieren imaging and design of the experiments 43

4.1 Introduction 43

4.2 Bubble cap film thickness 44

4.3 Deformation of thin films 46

4.4 Schlieren visualization 47

4.4.1 Bacteria and particles in bubbles 47

4.4.2 Particles in flat films 49

4.4.3 Rods in bubbles 50

4.4.4 Rods in flat films 51

5 Schlieren visualization: spot size to particle size ratio 55

5.1 Results and summary 57

6 Discussion and conclusion 59

List of Figures

1-1 Direct visualizations of different events at the origin of infectious droplets potentially responsible transmission through air and on surfaces. (*a*) Trajectory of mucosalivary fluid droplets expelled after a cough. (*b*) Fragmentation of mucosalivary fluid filaments into droplets following a sneeze. (*c*) Trajectory of droplets above a toilet bowl and created during the flush of a standard high-pressure hospital toilet. ($d - e$) Burst of a bubble at the surface of water contaminated with *E. coli* and ejecting droplets in the air. Reproduced from [1–4]. 16

1-2 On-shore wave breaking generates large numbers of bubbles. Bursting bubbles in turn generate sea sprays disseminated in the air we breath. The size of the bubbles generated govern the size and speed of the spray droplets created [5]. The composition of the droplets is determined by the composition of the bubble film. Picture credit L. Bourouiba. . . . 17

1-3 Mechanisms of generation of ocean spray, from bubble bursting (jet and film drops) to spume drops generated during wave-crest breaking. Rainfalls also contribute to bubble generation and bursting, and subsequent droplet emission [6]. 18

1-4 Representation of organic material inside and on the ocean Surface Microlayer (SML) [7]. 19

1-5 Film drops created from the burst of a bubble of radii on the order of 2-5 mm. The droplets emitted have a wide range of sizes and speeds which depend on the film thickness and properties at burst [1]. 21

2-1 A 22s-old bursting bubbles gives birth to numerous micro droplets. Scale bar 1 mm, 0.22 ms between each frame. 26

2-2 Life story of a bubble: (A) birth, (B) rise, (C) surfacing, (D) burst, (E) film drop production, (F) jet drop production. Reproduced from [8]. 27

2-3 (A) Film drops and (B) jet drops can be a vector for pathogens. Reproduced from [8]. 28

2-4 Through Schlieren photography (the upper part is the set up), we can see bacteria in a bubble film. The concentration of bacteria is about 5×10^8 cells/ml ($\mathrm{OD}_{600} = 0.470$) in DI water, the times are $t = 10$, 26, 29, and 36s. The corresponding bubble cap thickness are $h = 2.5$, 1.3, 1.1, and 0.9 μm. Scale bar is 1mm. Bacteria are observed at long lifetimes, when the bubble film reaches a thickness of the order of the bacteria size. 29

3-1 *E.coli* GFP O157:H7 giggling under the microscopy. The time between each frame is 0.21s, the scale bar is 2 μm. 32

3-2 *Echerichia coli* GFP O157:H7 with four different cell concentrations under microscope. The OD_{600} is: (1) 0.744, (2) 0.372, (3) 0.186, (4) 0.093. They produce strong green fluorescence when excited by blue light. Scale bar is 50 μm. 34

3-3 Measured *E.coli* growth curve using OD_{600} in LB medium. We can see that after 10 hours the concentration becomes stable 37

3-4 *E. coli* concentration as a function of the optical density at 600 nm (OD_{600}) in three different media: deionized (DI) water, and two other minimal solutions of salt: phosphate buffer (KP), and potassium phosphate buffer (PBS). 38

3-5 OD_{600} value of *E.coli* with five different initial concentrations. These time evolution show that *E. coli* in PBS do not grow, regardless of their initial concentration. 39

3-6 Bacteria phosphate buffer (KP) solution. From left to right, the concentration of bacteria increases, so that the transmittance of light decreases. However, surface tension changed little with concentration. Scale bar is 1 cm. 40

3-7 The surface tension of bacteria with different concentrations in different solutions. We can see that the concentration of bacteria will not change the surface tension of the solution in either PBS or KP. 41

4-1 *E. coli* in a bubble film. The concentration of bacteria is approximately 5×10^8 cells/ml in DI water. The times are t =10, 26, 29, and 36s. The corresponding bubble cap thickness are h = 2.5, 1.3, 1.1, and 0.9 μm. Scale bar is 1mm. Reproduced from [1]. 44

4-2 Measurement of the bubble cap film thickness. A needle punctures the film and creates a hole that recedes at constant speed U_c, related to the film thickness by Taylor-Culick relationship: $U_c = \sqrt{2\sigma/\rho h}$, where h is the film thickness, σ the surface tension and ρ is the density of fluid. 45

4-3 Bubble cap film thickness time evolution in deionized water inoculated with *E. coli* at OD_{600} = 0.474. Each point correspond to a single bursting bubbles. The longer bubbles stay at the surface, the thinner they are. 46

4-4 Particle entrapped in a thin liquid film of thickness h_0, which is smaller than the particle diameter $2r_p$. θ_c is the contact angle between the fluid in the film and the particles. Figure adapted from [9]. 47

4-5 Diagram of a Schlieren setup. Rays from an initial light sources go through 3 lenses and a pinhole to generate parallel beams. In the test area, light is deflected when it encounters a change of optical index, such as when going through a bubble. The beam are then refocused on the sensor of a camera. 48

4-6 Numerical Schlieren visualization of a meniscus around a particle in a thin film (a). After parallel light goes through the meniscus, the Schlieren optical setup (b) acts as a magnifier: the trace of the particle on the camera sensor (c) is larger than the particle itself. Schlieren images of menisci from experiments (d) show a very good agreement with the simulation (Scale bars: 100 μm). 49

4-7 Particles in a flat soap film. The upper one is particle with diameter $= 0.5$ μm, the lower one is particle with diameter $= 2$ μm. Scale bar is 1 cm. g is the direction of gravity. 50

4-8 Copper rod going through a bubble. We can observe a meniscus profile around it. d is the diameter of the rod, D is the diameter of the meniscus profile. $d = 260\mu$m, $D = 2.33$ mm. 51

4-9 Schlieren radius ($R_{meniscus}$) of steel rods with different diameters as a function of time. 52

4-10 When a cylindrical needle is placed in a soap film, we can observe a meniscus profile around it (left down). After the film bursts, the meniscus profile disappears (right down). d is the diameter of the rod, D is the diameter of the meniscus profile. $d = 137\mu$m, $D = 1.87mm$. . 53

5-1 The set up of the Copper Ring frame. We used 1mm diameter copper wire to make the ring frame. 56

5-2 The diameter of yellow copper rods were measured under the microscope. 56

5-3 Contact angle measurement. θ_1 and θ_2 are the two contact angles, measured using a in-house precise image processing code 57

5-4 Schlieren spot diameter as a function of the rod diameter. Results from experiments (colors) and simulations (black) are represented. CA refers to contact angle. 58

List of Tables

3.1 The pH evolution of *E.coli* with four different initial concentrations. The pH did not change a lot 38

Chapter 1

Chemical, particle, and pathogen transfers

Despite widespread vaccination programs, the healthcare and economic burdens of respiratory diseases remain enormous. Influenza returns every year, SARS and MERS are growing concerns, and the threat of emerging and re-emerging pathogens to the global population is growing. In this context, understanding the dynamics of pathogen transfer from one host to the next directly or indirectly via contamination of water or surfaces is critical to improve the modelling of epidemics and ultimately to develop efficient mitigation strategies [10–12]. Nevertheless, the transmission mechanisms of even the most common diseases remain poorly understood.

Droplets and droplet nuclei carrying chemicals, spores, viruses, and bacteria can be created directly from an infected or contaminated host, such as from respiratory events such as coughs, sneezes, talks, or laughs [2, 13]. The distance over which respiratory droplets can be transmitted depends on their size and on the properties of the sneeze or cough cloud produced, it can range from 1 m to the entire length of a hospital ward [2, 3, 14]. They can also originate from contaminated water bodies [8]: sea and ocean sprays [15], wastewater plants [16, 17], sewage [18], pools and hot tubs [19, 20], or flushes in indoor lavatory systems [4], as illustrated in figure 1-1. Droplets originating from contaminated water pools have been directly linked to respiratory diseases through the release of droplets in the air. This can be caused by various

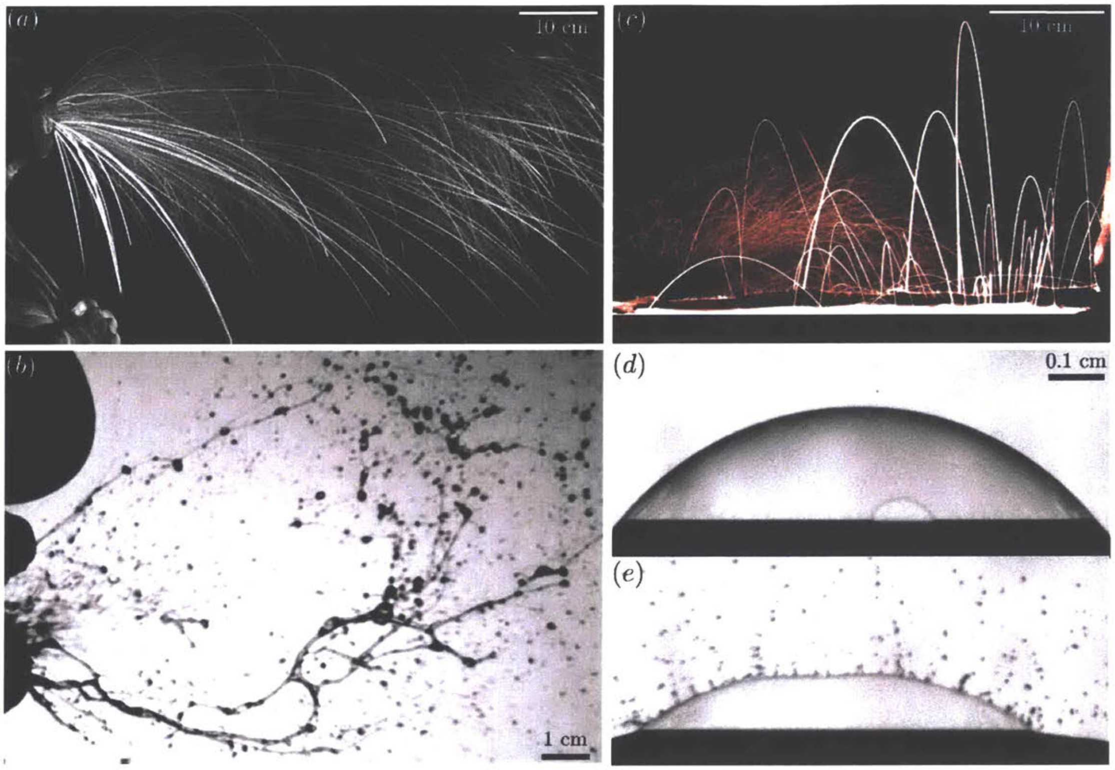

Figure 1-1: Direct visualizations of different events at the origin of infectious droplets potentially responsible transmission through air and on surfaces. (*a*) Trajectory of mucosalivary fluid droplets expelled after a cough. (*b*) Fragmentation of mucosalivary fluid filaments into droplets following a sneeze. (*c*) Trajectory of droplets above a toilet bowl and created during the flush of a standard high-pressure hospital toilet. $(d-e)$ Burst of a bubble at the surface of water contaminated with *E. coli* and ejecting droplets in the air. Reproduced from [1–4].

fragmentation processes, among which bursting bubbles (figure 1-1(d, e)) is the most ubiquitous and has been shown to be very efficient at transferring pathogens from infected water to the air we breathe [15].

In the environment, bubbles produce spray. Ocean spray droplets play a key role in the ocean-atmosphere physical and biochemical exchange. This exchange is critical in the dispersal of organic, inorganic, and biological compounds in this atmospheric boundary layer, which in turn can shape chemical reactions and physical processes in the atmosphere. When fully or partially evaporated, droplet-residues become solid particles that can promote cloud drop or ice nucleation and precipitation. In fact, such sprays can reside in the atmosphere for days transported in various forms. Spray

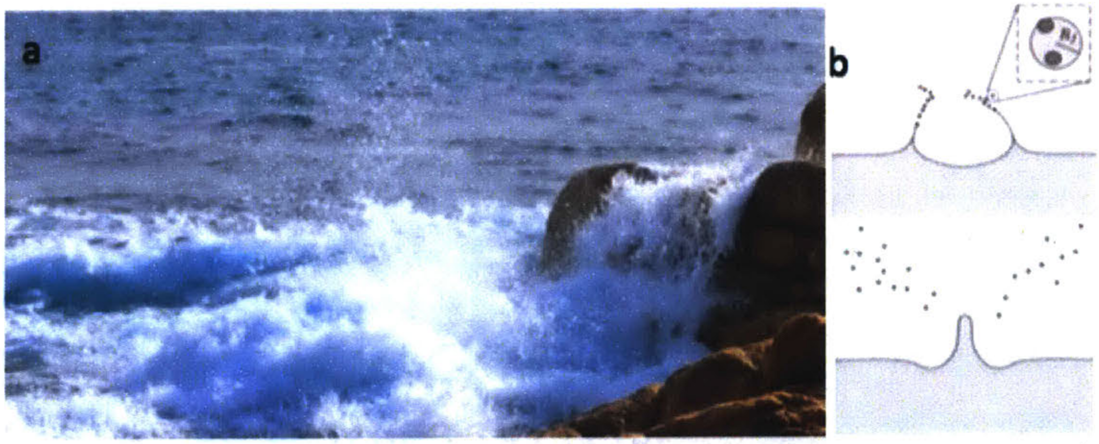

Figure 1-2: On-shore wave breaking generates large numbers of bubbles. Bursting bubbles in turn generate sea sprays disseminated in the air we breath. The size of the bubbles generated govern the size and speed of the spray droplets created [5]. The composition of the droplets is determined by the composition of the bubble film. Picture credit L. Bourouiba.

drops also play a key role for the dispersal of ocean organisms. They can furthermore contribute to changes in the thermodynamics and heat-exchange in the atmosphere, which in turn can have important feedback on the ocean dynamics itself (e.g., hurricane formation). Despite numerous attempts to sample and quantify sea spray to better estimate its effect on local and global climate and sea-atmosphere exchanges, our understanding of sea sprays and their complex formation and dissemination processes remains very limited. Wave breaking and rain can both lead to spray formation by inducing the formation of bubbles of a range of sizes that can re-surface and burst, thus projecting either jet or film drops depending on the size of the bubbles (Figure 1-2). Other effects such as spums of fluid sheared off by wind from wave-crests can also produce sprays (Figure 1-3).

Here, our focus is on the role of bubble bursting as it remains a major contributor to the formation of ocean sprays. Despite recent work on spray from bubble bursts, the results remain confined to highly idealized studies of pure water, soapy or highly viscous bubbles, thus severely limiting the relevance of the results for the oceans. Moreover, the effects of environmental, chemical, and biological conditions on bubble-bursting and resulting spray is a complex problem with entangled factors that have

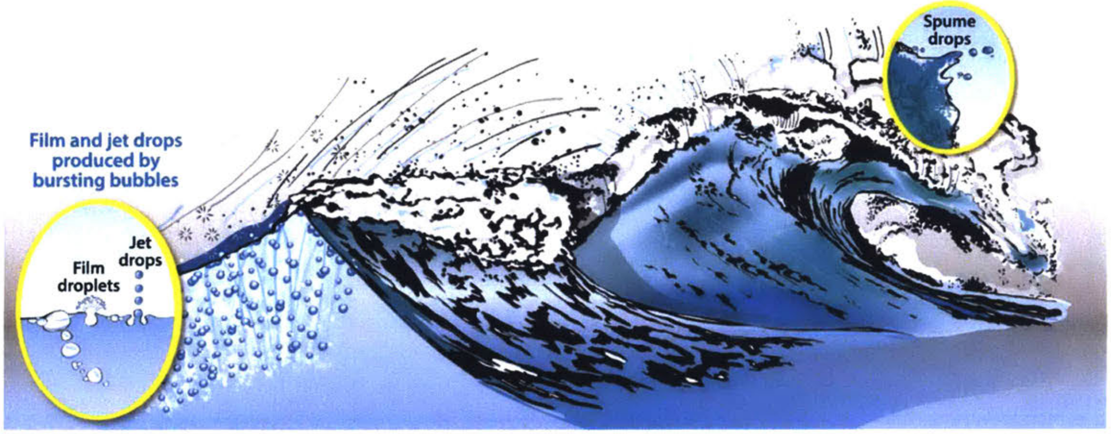
Film and jet drops produced by bursting bubbles
Jet drops
Film droplets
Spume drops

Figure 1-3: Mechanisms of generation of ocean spray, from bubble bursting (jet and film drops) to spume drops generated during wave-crest breaking. Rainfalls also contribute to bubble generation and bursting, and subsequent droplet emission [6].

so far been difficult to parse out. A recent comprehensive review of research on Ocean Spray by Veron [6] identified seven key future issues and needs in research in ocean spray, including *"Small film and jet droplets transport significant amounts of organic matter and inorganic chemical species. It is likely that the size-dependent biochemical compositions need to be included in the source functions for the smallest droplets to better estimate their aggregated impact on the global aerosol cycle"*. However before even examining the composition of the droplets, one key question remained undressed: the dynamics of enrichment of the bubbles as they move up the water column and surface.

1.1 Bubbles and contaminants

Presence and transport of organic and inorganic particles at the oceanic liquid-air interface (Figs. 1-2, 1-3) play a vital role in sustaining marine ecology and impact climate, making the study of these phenomena of extreme relevance in oceanography [6, 21–30]. This liquid-air boundary layer is typically 40-100 microns thick and is therefore also known as the Surface Microlayer (SML). It contains chemical and biological materials, and its importance can hardly be overestimated, given that it occupies more than 70% of the Earth's surface. It is the medium for dispersal of con-

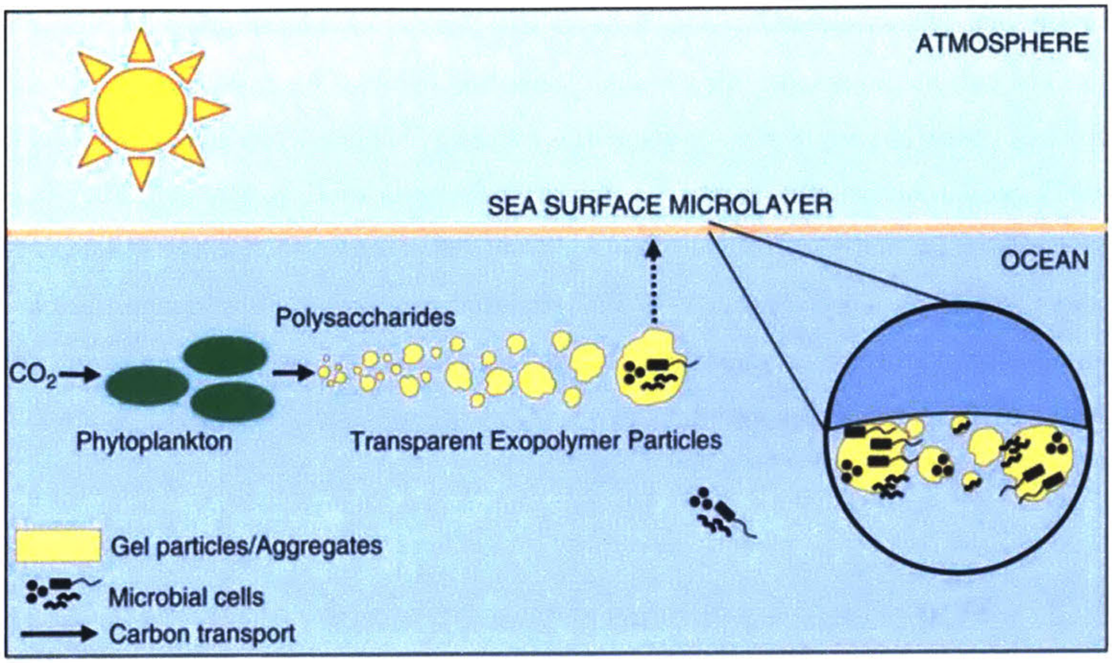
ATMOSPHERE
SEA SURFACE MICROLAYER
OCEAN
Polysaccharides
CO₂
Phytoplankton
Transparent Exopolymer Particles
Gel particles/Aggregates
Microbial cells
Carbon transport

Figure 1-4: Representation of organic material inside and on the ocean Surface Microlayer (SML) [7].

stituents of bulk ocean water to the atmosphere and therefore serves as a crucial link between aquatic life in the ocean water and the overlying air. For instance, through diffusion, convection or advection, sea-spray aerosols formed at the SML catapult organic materials from the oceans to the troposphere where they can act as nucleating agents for ice and cloud formation [21]. These processes therefore have significant implications for local and global precipitation levels. Understanding and accurately modeling these SML processes from the viewpoint of the relevant hydrodynamic interactions at the ocean surface can therefore lead to more accurate and effective climate and weather modeling, prediction, and control or mitigation in times of detrimental or toxic chemical or biological pollutants or invasions of the oceans/seas/coastal regions [21, 31]. Besides the impact on climate, weather, and radiative transfers, the biogeochemical exchange serves as a mechanism for nourishment to many life forms on and below the water surface. The SML is therefore especially critical to the marine ecosystem (Figure 1-4). The microbial and chemical transport that occurs in the SML can also affect human populations onshore, especially in the vicinity of lakes and oceans [22, 24, 32–36].

The rich lifeforms make up a biofilm consisting of algae, bacteria and viruses and form an integral part of the marine surface ecology. This micron sized layer is also the home for various autotrophs, ranging from bacteria to algae [37, 38]. They help in nutrient, O_2 and CO_2 transport to and from the ocean surface to the atmosphere and also affect energy transfer [39]. Bacterial and algal neustonic communities have the potential to serve as important transfer sites, either accelerating or slowing the fluxes of elements or compounds between the atmosphere and the water column and vice versa [40].

1.2 Water-air exchanges via bubbles

Winds also play a pivotal role in convection of sea sprays and their particulate residues over large distances [23, 25, 41, 42]. Microbial transport is greatly aided by strong winds [41], given breaking waves and spumes that occur; while the presence of oil slicks dampens the effects of winds and thus inhibits energy transfer and mass transport across the SML. Accurate physically-rooted mathematical modeling of these important factors is required to improve our assessment of the spread of chemical and biological organisms and contaminants. Two particular mechanisms that are highly efficient in these exchanges are: bubble movement through the water bulk; and bubble bursting at the liquid-air interface [8, 21, 23, 43, 44]. The latter generates a large range of sizes of droplets as illustrated in Figure 1-5 and is part of the focus of this thesis.

Woodcock [45] was the first to observe that bubbles originating from waves generate infected droplets causing acute respiratory illness. Many other case studies report a link between infected water bodies, bubble bursting, and respiratory illness [8, 15]. One of the main mechanisms that has been proposed to explain the rich concentration of contamination in droplets when compared to the bulk concentration is that a bubble scavenges contaminants on its way as it rises through the water column (See Fig. 1-3) [46–48]. However, the discrepancy in the measurements carried out in these

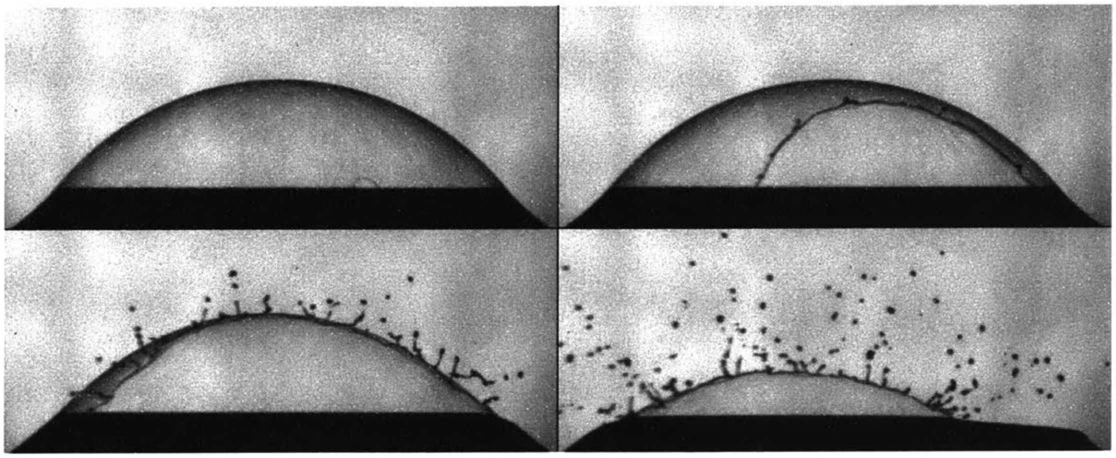

Figure 1-5: Film drops created from the burst of a bubble of radii on the order of 2-5 mm. The droplets emitted have a wide range of sizes and speeds which depend on the film thickness and properties at burst [1].

studies do not allow for a clear mechanism to emerge or be validated [48, 49].

1.2.1 Physiology of a bubble

At the end of its travel through a water bulk, a bubble reaches the air-water interface forming a thin liquid film, a bubble cap, which encapsulates the air cavity. Competing gravitational and interfacial forces select the bubble equilibrium shape [50, 51]. The capillary length $\ell_c = \sqrt{\sigma/\rho_w g}$, on the order of the millimeter for air-water interfaces, is the length scale at which these forces balance; with σ the water surface tension, ρ_w the water density, and g the gravitational acceleration. For small Bond number $\mathrm{Bo} = (R/\ell_c)^2$ bubbles remain mostly submerged and spherical, while buoyancy drives larger bubbles to extend further into the air. Bubbles smaller than $\mathcal{O}(\ell_c)$ remain mostly submerged and spherical, while buoyancy drives larger ones to extend further into the air against surface tension.

All bubbles eventually burst. Their cap radius R, which measures their cap shape and extension above the water surface, selects the mechanisms of their ageing, burst, and the outcome of such burst [1]. A single bursting surface bubble can generate hundreds of such film drops (figure 1-5). While bubbles responsible for film drops are suspected to be less numerous than those responsible for jet drops at the surface of oceans [52], most sea surface droplets are nevertheless thought to originate from film drops [53–55]. For relatively clean water interfaces, and for bubbles for which gravitational drainage can be neglected (an assumption valid for $R \lesssim 5\ell_c$), the number N and mean diameter $\langle d \rangle$ of film drops are estimated to be controlled by the bubble cap radius R and film thickness at burst h_b as $N \sim (R/\ell_c)^2(R/h_b)^{7/8}$ and $\langle d \rangle \sim R^{3/8}h_b^{5/8}$ [56].

What sets the concentration of organisms of chemicals or particles in these droplets is not known. Although the dynamics of scavenging of biological or chemical agents during the rise of the bubble can play a role, another neglected piece of this problem is the dynamics at the interface after the bubble has surfaced (Figure 1-5). In fact, the mechanism that triggers bubble rupture and is responsible for the selection of droplet sizes and speeds remains little understood. Indeed, since 1966 it has been thought that the thin film cap forming bubbles at the interface simply drains and thins until burst. The dynamics of the burst is governed by a rich interplay of film thinning and interaction with local surfactant or particles and a coupling with the air surrounding the bubble as recently discussed in [1]. The dynamics of the thinning and burst is rich, but remain outside of the scope of this thesis. In this thesis, our focus is on the development of a method for visualization of contaminated bubble caps after they surface. We aim to develop a method to quantify directly the dynamics of interaction between the contaminants, particles or organisms, and the film they are trapped in.

1.3 Overview of the project

In this chapter, we briefly introduced the essential role that contaminated droplets can play in the environment and health. We introduced the important role of bubbles in the environment and their role in coupling the content of water (good or bad) with the air we breathe. We also introduced some key concepts relevant to bubble life and death that contribute to this process of water-to-air transfer. However, key questions remain unknown. The central question on which we focus is the dynamics of contaminated bubbles at the interface. In this thesis, we focus on developing and validating a technique and model to directly visualize and quantify the contaminants on bubble interfaces during their life at the surface. In terms of contaminants, in this thesis, we will consider a combination of biological agents such as *Escherichia coli* and artificial agents, such as solid particles and rods of a range of wetting and surface properties.

In the first part (chapters 2), we focus on observing particles in bubbles. Bubbles are small, and the particles inside bubbles are even smaller. We used a visualization method called Schlieren imaging to visualize for the first time particles and bacteria in bubbles. In Chapter 3, we discuss our biological methodology for preparation of a range of solutions to test the efficacy of this method to visualize organisms and under which conditions. In Chapter 4, we discuss the theoretical models at plan that can explain our visualization quantitatively. In Chapters 4-5, we discuss a series of analog experiments involving particles, rods, and bacteria coupled with bubbles and thin vertical films aiming to validate the calibration from Schlieren spot observed to particle size or intrusion in the thin interface. Finally we discuss the next steps and implication of our results in Chapter 6.

Chapter 2

Bubbles and contamination

2.1 Bubbles in contaminated water

In nature, bubbles are considered to be critical in exchanging materials from water to the air [8, 57]. Sea spray, produced by bursting bubbles, plays an essential role in transporting chemicals, viruses, and bacteria [15, 58] from the oceans to the atmosphere. Waterborne diseases, caused by pathogens in contaminated water for instance from in sewage, toilets, pools, or tap water may also be transmitted by aerosols generated by bubbles [59]. Bubbles burst after they arrive at the surface of a liquid, forming an entrapped air cavity which rapidly collapses [60]. When a bubble bursts, it generates droplets (Figure. 2-1) which disperse what was contained in the bulk water [57].

Woodcock (1948) recognized that droplets ejected by bubbles from the sea shore can cause respiratory diseases [61, 62]. Harold (1974) suspected that bursting bubbles eject microalgae into the air, causing allergies and respiratory illnesses [63]. Higgins (1964) tested the aerosol produced by bursting bubbles created by water contaminated by different bacteria, and found that the concentration of some species (e.g., *S. marcescens*) in the droplets was higher than in the water bulk [64]. Blanchard and Syzdek (1970) showed that the concentration of bacteria in the droplets created by bursting bubbles can be up to a thousand time greater than in the bulk water [15, 33, 65].

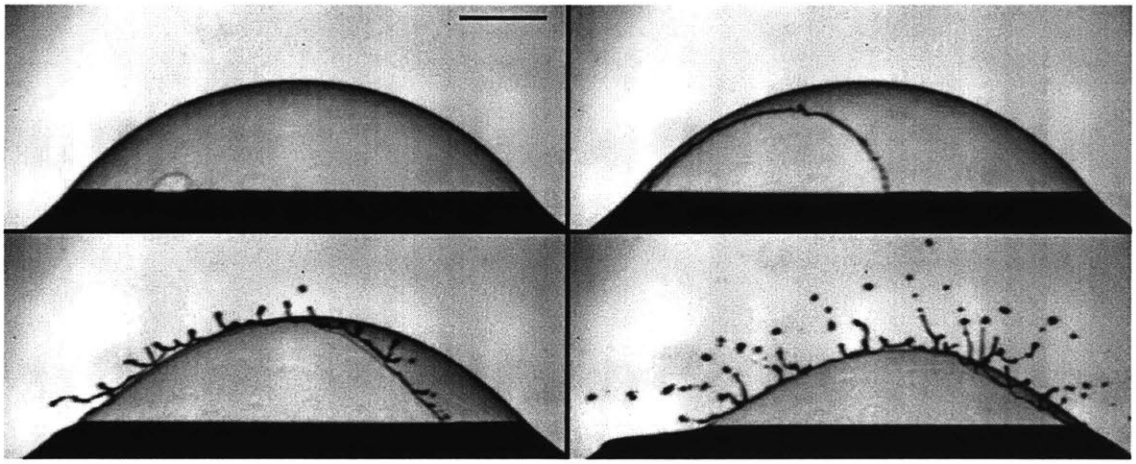

Figure 2-1: A 22s-old bursting bubbles gives birth to numerous micro droplets. Scale bar 1 mm, 0.22 ms between each frame.

Microbial aerosols produced by sewage treatment plants have also been suspected to cause health issues for plant workers and nearby residents, as they disperse viruses, bacteria, and other pathogens [66]. High concentration of bacteria can be found in wastewater treatment plants [67], estuarine water [68], and other places. The density of bacteria in the surface is higher than in the bulk water because of the formation of microlayers [34].

2.2 Bubbles and pathogens

Bubbles are ubiquitous and understanding their role in droplet production requires an understanding of their physics. In this section, we will discuss the physical principles ruling the life of bubbles.

Bubbles can be created for instance by strong flows that blend air into water [69], by rain [33], or from dissolved gases or rapid changes of pressure via cavitation [57]. Once formed, bubbles move upward due to their buoyancy. Rising bubbles interact with the surrounding fluid [8]: they can capture particles and pathogens along their trajectory. The process through which bubbles collect particles on their surface is called *scavenging* [70]. Scavenging can result in an increase in concentration of bacteria or particles on the surface of bubbles [71]. Some materials and organisms have

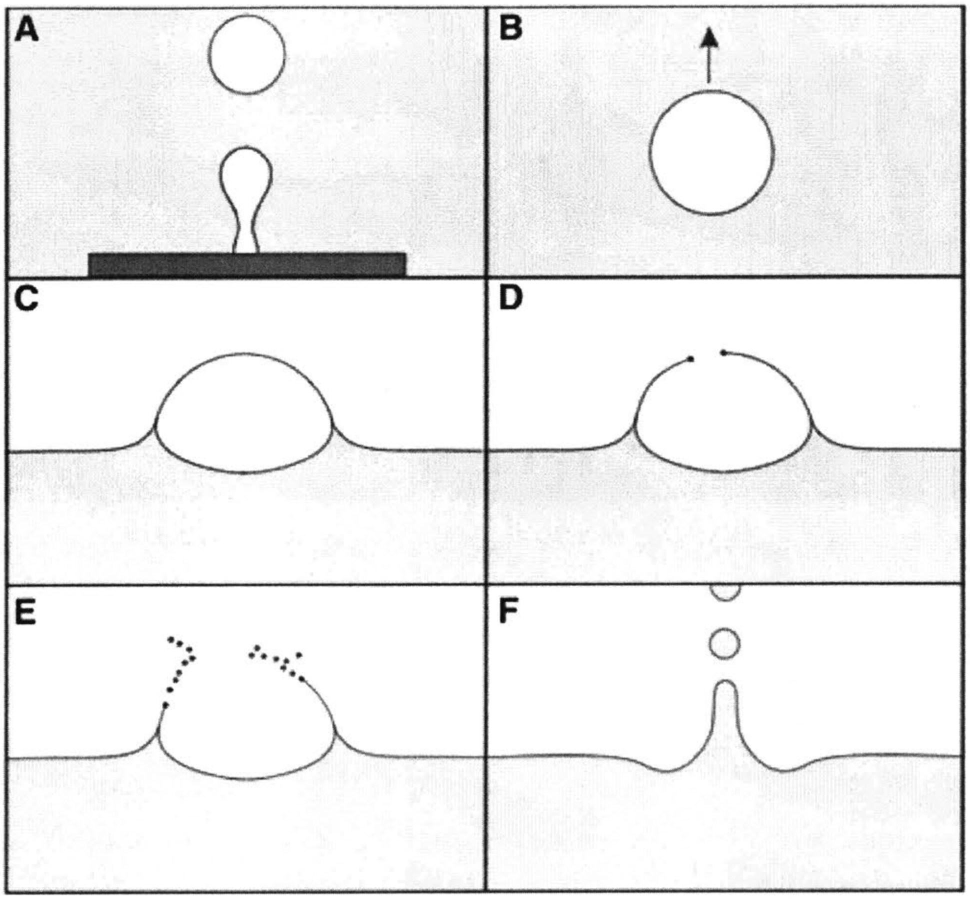

Figure 2-2: Life story of a bubble: (A) birth, (B) rise, (C) surfacing, (D) burst, (E) film drop production, (F) jet drop production. Reproduced from [8].

abundant hydrophobic sites and are particularly good candidate to be scavenged by rising bubbles [65]. When a bubble surfaces, its shape is defined by the competition between gravity and capillarity. The liquid in the bubble film drains into the bulk water, the film becomes thinner until it ruptures [8]. Bursting bubbles create two types of drops [72]. The first set of droplets are called *film drops*: they are created from the bubble cap film which separates the inside of the bubble from the air above it (Figure 2-2 -E). The second set of droplets are called *jet drops*, which are generated later from the liquid jet following the film rupture (Figure 2-2 -F). Bursting of relatively large bubbles (greater than 1 mm in diameter) mainly creates *film droplets* [73]. These droplets can transport pathogens (Figure. 2-3) [8].

The bacterial enrichment factor (EF) is the concentration of bacteria in drops

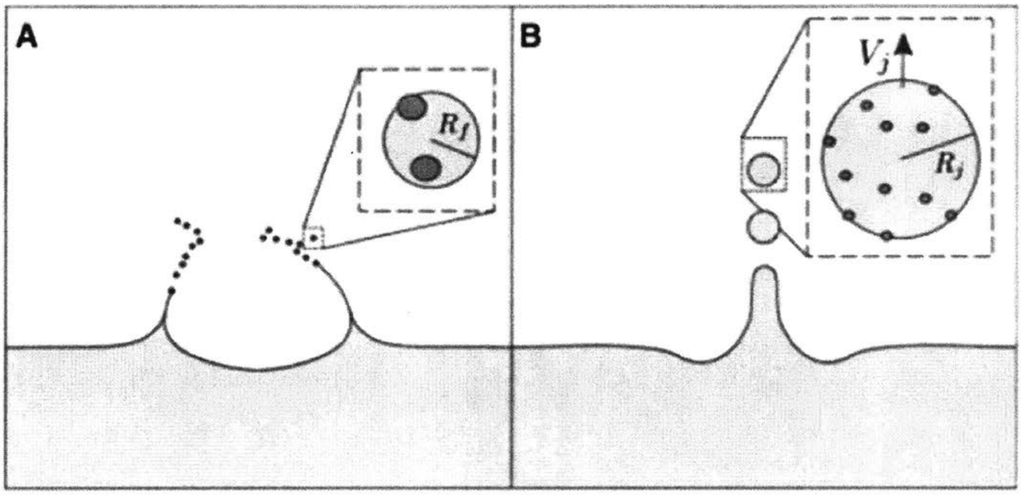

Figure 2-3: (A) Film drops and (B) jet drops can be a vector for pathogens. Reproduced from [8].

when they are produced divided by their concentration in the water where the bubble was formed [65]. It is usually greater than 1: droplets from bubbles are highly concentrated in bacteria. Three parameters are believed to control enrichment[15]: 1) the mechanisms of bubble scavenging, 2) the type of bacteria, and 3) the droplet size, and 4) the drop position in the jet set. Bubble scavenging, as introduced in the previous paragraph, happens when bubble rise in the water. The volume of bacteria collected by a bubble can be described as a function of bubble rise distance, which is the height that a bubble rises through the water [15]. Bacteria follow the streamlines close the bubble, contact with the bubble, and are scavenged [70]. Prior studies showed that there exists a maximum EF in a certain jet drop diameters and the EF decreases from the top to the bottom of a jet set [65]. However, we cannot create an estimation of EF from one study to another. There is no clear understanding of what parameters shape the composition of film drops. Because these droplets originate from the bubble cap film, to understand them we first need to understand the bubble cap and its composition.

In this thesis, we focus on developing a method of observation of particles within the bubble cap to gain fundamental insights into the mechanism of pathogen dissem-

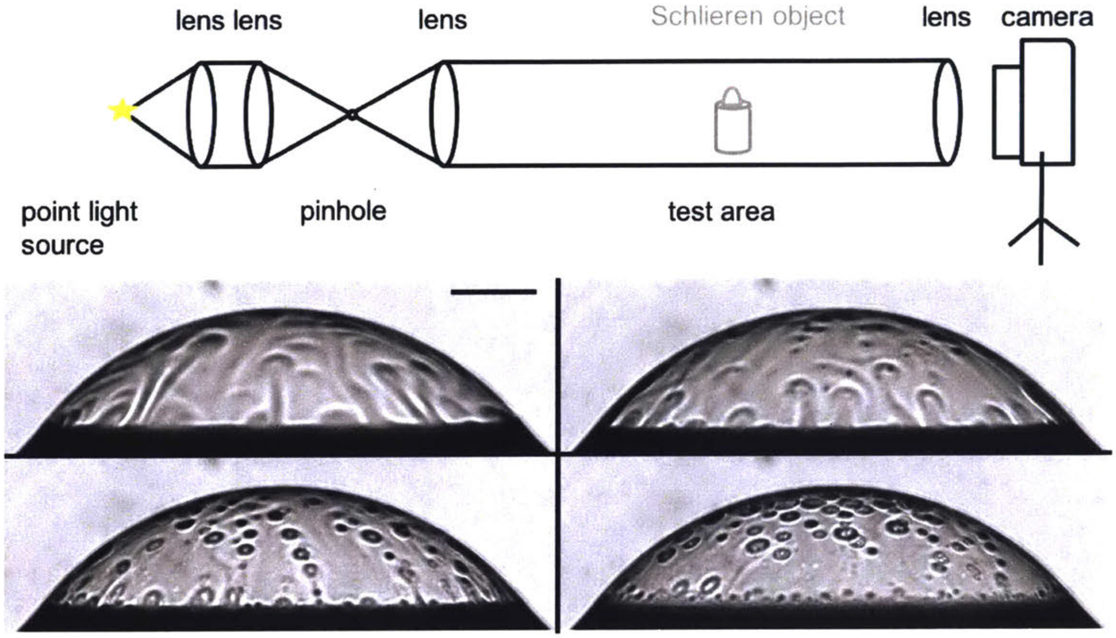

Figure 2-4: Through Schlieren photography (the upper part is the set up), we can see bacteria in a bubble film. The concentration of bacteria is about 5×10^8 cells/ml ($\mathrm{OD}_{600} = 0.470$) in DI water, the times are $t = 10$, 26, 29, and 36s. The corresponding bubble cap thickness are $h = 2.5$, 1.3, 1.1, and 0.9 μm. Scale bar is 1mm. Bacteria are observed at long lifetimes, when the bubble film reaches a thickness of the order of the bacteria size.

ination and droplet enrichment from bursting bubbles. Indeed, figure 2-4 is a striking illustration of visualization of bacteria in bubbles.

2.3 Summary

Bubbles are ubiquitous and they play critical roles in transporting materials from liquid to air. Air bubbles that move upward to the surface can collect organic and non-organic particles during their journey. When they burst at the surface, they produce film drops and jet drops, and the concentration of bacteria, viruses, or particles in these drops can be several hundred times higher than in the bulk water. Understanding how microorganisms or particles are enriched in bubble caps is very important to gain insight into the mechanism of water-born pathogen dissemination and to control it. In this thesis, we focus on developing a method of observation of particles within the bubble cap to gain fundamental insights into the physics of bubble enrichment and air contamination by them.

Chapter 3

Biological background

We used *Echerichia coli (E. coli)* GFP O157:H7 attenuated laboratory strains as the mock pathogen for this study. This chapter starts by introducing the protocols associated with the preparation of these bacteria. We chose *E. coli* as model organisms to illustrate the dynamics of contamination because it is one of the most ubiquitous and studied bacteria. We note that, in contrast, the body of work of Blanchard and Syzdek [15] on bacteria and bubbles was performed with *S. marcescens.* In the second part of this chapter we also evaluate the effect of bacteria in a range of concentrations on water properties, namely its surface tension, which is key for the life of bubbles at the interface. In fact, we find little effect, yet this might not be the full picture and subtle changes in surface tension might still have important effects as discussed at the end of this chapter.

3.1 Bacteria protocol

3.1.1 *Echerichia coli*

Echerichia coli (*E.coli*) are bacteria widely found in the environment, food, and intestines of animals. Most *E.coli* strains are harmless, but some serotypes are associated with severe human diseases, among which O157:H7 is the most prevalent in North and South America and in the UK [74, 75]. *E. coli* O157:H7 is one of the

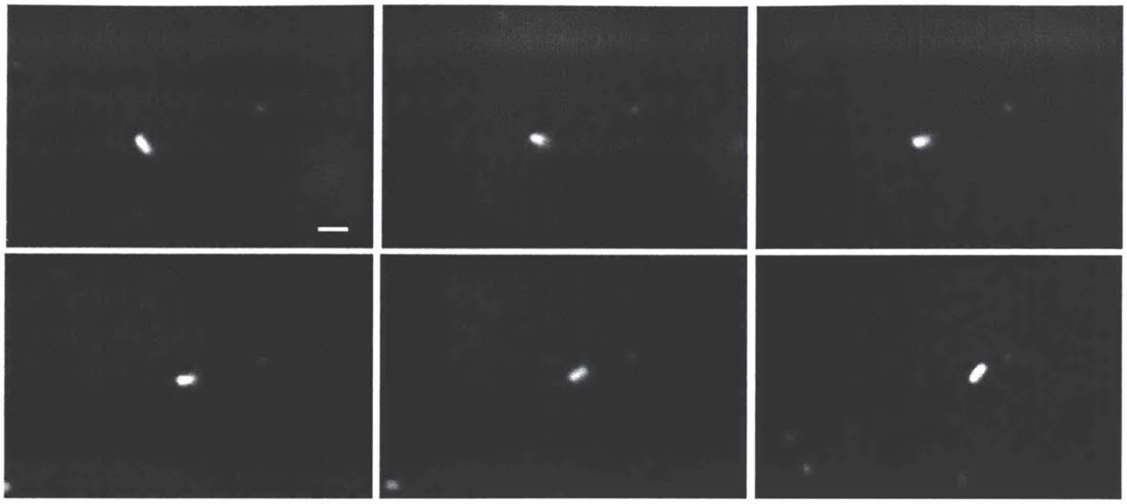

Figure 3-1: *E.coli* GFP O157:H7 giggling under the microscopy. The time between each frame is 0.21s, the scale bar is 2 μm.

Shiga–toxin–producing types of *E. coli*, which can cause diarrhea, hemorrhagic colitis, and hemolytic uremic syndrome [75]. In our project, we used *E.coli* Biosafety level 1 (BSL-1) [76] attenuated laboratory strain. A microscopic visualization of *E. coli* is shown Fig. 3-1.

3.2 Methodology

3.2.1 Bacterial Culture

E.coli are cultured in Luria broth (LB) media with ampicillin 100mg/ml added to prevent the growth of other bacteria. LB is a nutrient-rich medium commonly used to culture bacteria in the lab. The addition of agar to LB results in the formation of a gel that bacteria can grow on, as they are able to gather nutrition from LB within the agar but cannot digest agar.

Plasmids can carry one or more antibiotic resistance genes, which confer resistance to a specific antibiotic to the bacteria carrying them. The presence of an antibiotic resistance gene on a plasmid allows to easily isolate bacteria containing that plasmid from bacteria. The addition of an antibiotic to the medium allows for the selection of only those bacteria with specific antibiotic resistance, which is usually conferred by a plasmid carrying the antibiotic resistance gene. The *E.coli* ampicillin resistance gene, whose nucleotide sequence is pBR322, encodes a penicillin β-lactamase [77]. Ampicillin is a β-lactam antibiotic that can kill Gram-positive and some Gram-negative bacteria. It almost does not affect the growth of *E.coli* when the concentration is appropriate and will delay the log phase when the concentration is relatively high [78]. Therefore, we add ampicillin in an appropriate volum to the LB media, so as to prevent the growth of other bacteria and not delay the growth of *E.coli.*

3.2.2 Protocols to make LB agar

The protocol to make 1L of LB agar (makes about 50 LB agar plates):

1. Weight out the following into a 1L Erlenmeyer flask: 10g NaCl, 10g Tryptone, 5g Yeast Extract, 15g Agar. And add deionized water to 1L.
2. Swirl to mix.
3. Cover the top of the bottle and lable with autoclave tap.
4. Autoclave on the liquid setting for 40 minutes.
5. After removing the solution from the autoclave, put them into water-bath to cool to 55 °C.
6. Add Ampicillin 100 μg/mL to the solution and swirl to mix.
7. Keep your bench area sterile by working near a flame or bumsem burner.
8. Pour 20mL of LB agar per 10cm polystyrene Petri dish.
9. Place the lids on the plates and allow them to cool until solidified, then invert the plates.
10. Label the agar plates and store them in plastic bags at 4 °C.

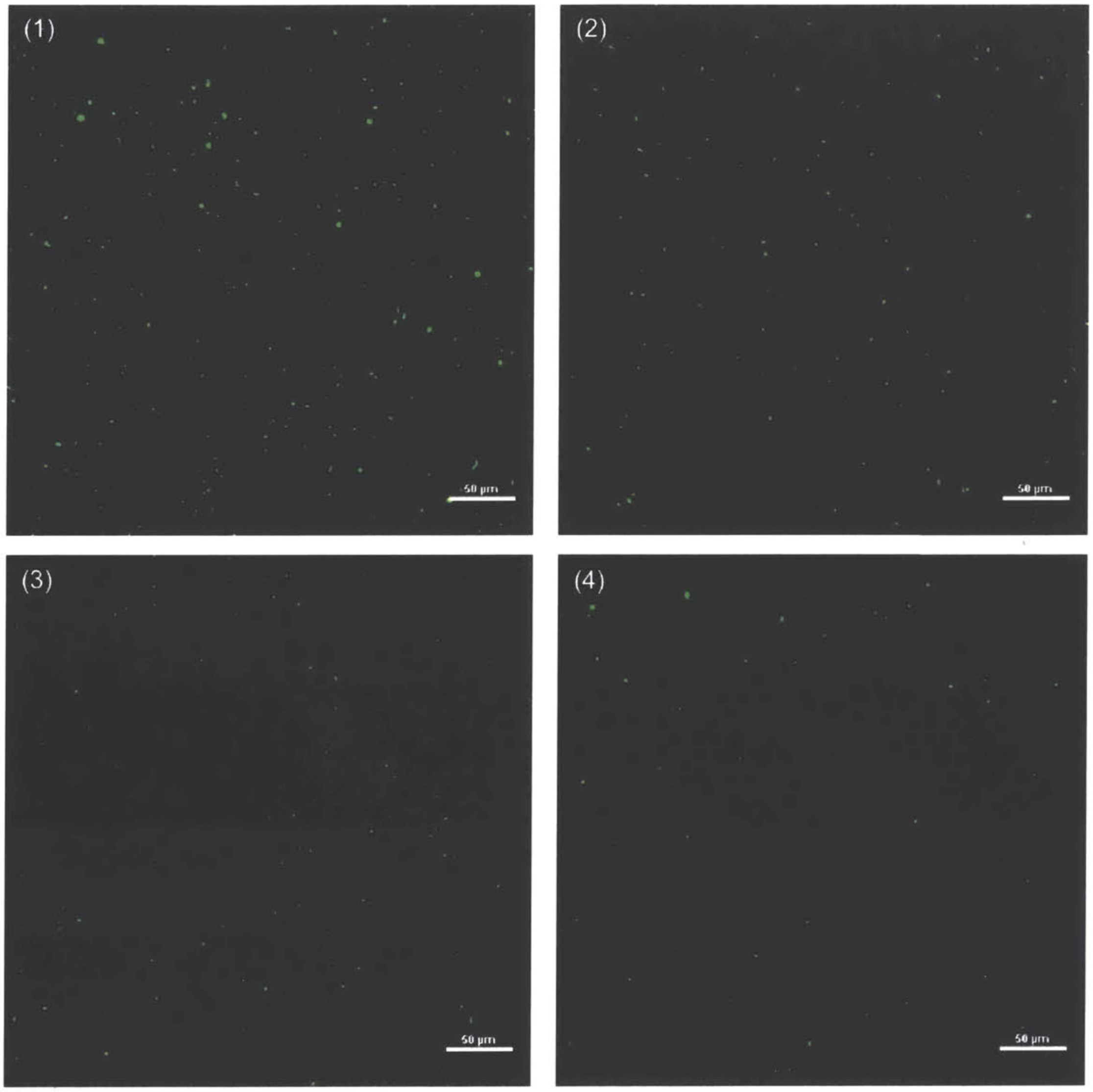

Figure 3-2: *Echerichia coli* GFP O157:H7 with four different cell concentrations under microscope. The OD_{600} is: (1) 0.744, (2) 0.372, (3) 0.186, (4) 0.093. They produce strong green fluorescence when excited by blue light. Scale bar is 50 μm.

3.2.3 *E.coli* culture from -80 °C freezers

Culture bacteria from glycerol stocks

1. Take *E.coli* from -80 °C freezers, put them in ice/ dry ice.
2. Keep your bench area sterile by working near a flame or bumsem burner.
3. Label the bottom of the plate with the plasmid name, the date, the antibiotic resistance, your name.
4. Using a sterile inoculate tube, touch the bacteria growing within the punctured area of the stab culture or the top of the glycerol stock.
5. Gently spread the bacteria over a section of the plate.
6. Incubate plate with newly plated bacteria for 24 hours at 37 °C.
7. In the next day, colonies should be visible. A single colony should look like a white dot growing on the solid medium. This dot is composed of millions of genetically identical bacteria that arose from a single bacterium.

Inoculating a liquid bacterial culture

1. Using an inoculate tube, a sterile pipette tip or toothpick, select a single colony from your LB agar plate.
2. Drop the tip or toothpick into the liquid LB + antibiotic and swirl.
3. Loosely cover the culture with a cap that is not air tight, or leave at least half of the tube with air.
4. Incubate bacterial culture at 37 °C for 8 - 10 hours (in the exponential phase according to the growth curve) in a shaking incubator.
5. Measure the OD curve of the bacteria

Creating Bacterial Glycerol Stocks

Bacterial glycerol stocks are important for long-term storage of plasmids. If you freeze the glycerol stock tube at -80 °C. The stock will be stable for years.

1. Follow the steps in Section 3.2.3.
2. Make the 50% glycerol solution by diluting 100% glycerol 1:1 in dH20.
3. After you have bacterial growth, add 500 μL of the overnight culture to 500 μL of 50% glycerol in a 2 mL screw top tube and gently mix.
4. Shake the tube to make sure no bubbles in the mixed solution.
5. Put the tube in the dry ice as soon as possible and move them to the -80 °C freezer.
6. To recover bacteria from the glycerol stock, open the tube and use a sterile inoculate tube to scrape some of the frozen bacteria off of the top and follow the steps in Section 3.2.3. Do not let the glycerol stock unthaw!

We measured the growth curve of *E.coli* and found that the concentration of bacteria in LB media saturates at OD_{600} equal to 0.654 (Table. ??) after 8 to 10 hours (Figure 3-3). OD_{600} is the absorbance of a sample measured at a wavelength of 600 nm. It is a common method for estimating the concentration of bacterial in a liquid and indicating the stage of cultured cell population [79]. To guarantee the quality of bacteria (prevent the generation of old cells and death cells), we used fresh bacteria typically cultivated for 10 hours.

3.2.4 Purification

When bacteria solutions is needed, first LB medium is washed of to ensure not duplication in the solution used. We wash bacteria with minimal medium two times by centrifugation (10 mn at 5000 rpm), then they are resuspended in deionized water or other media. Indeed, we also investigated two minimal media: phosphate-buffered

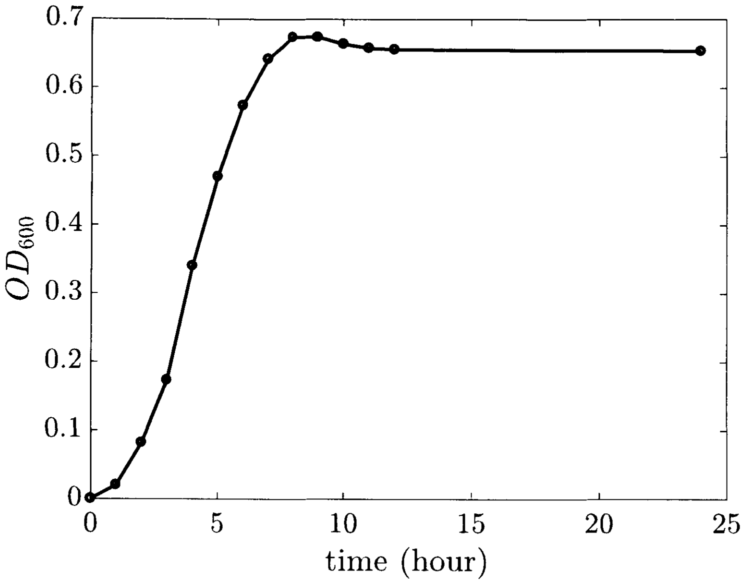

Figure 3-3: Measured *E.coli* growth curve using OD_{600} in LB medium. We can see that after 10 hours the concentration becomes stable

saline (PBS) and phosphate buffer (KP). PBS is a water-based salt solution containing disodium hydrogen phosphate and sodium chloride. Second, the bacteria solution was diluted use spectrophotometry (OD_{600} measurements) to estimate and adjust the concentration of bacteria.

We used a C-chip hemacytometer to count the cell concentration of *E.coli* in different solutions and at different OD_{600} (Figure 3-4). As expected, the relationship between OD_{600} and cell concentration is linear in a wide range of concentration.

3.3 Behavior of the bacteria liquid

3.3.1 OD and pH evolution

In order to observe the behavior of bacteria in the new solution, we measured the evolution of OD_{600} and pH of bacteria solution in different concentrations. The results show that OD_{600} and pH remain stable within 24 hours (Fig. 3-5, Table.3.1), which means the bacteria will not duplicate in the minimal media.

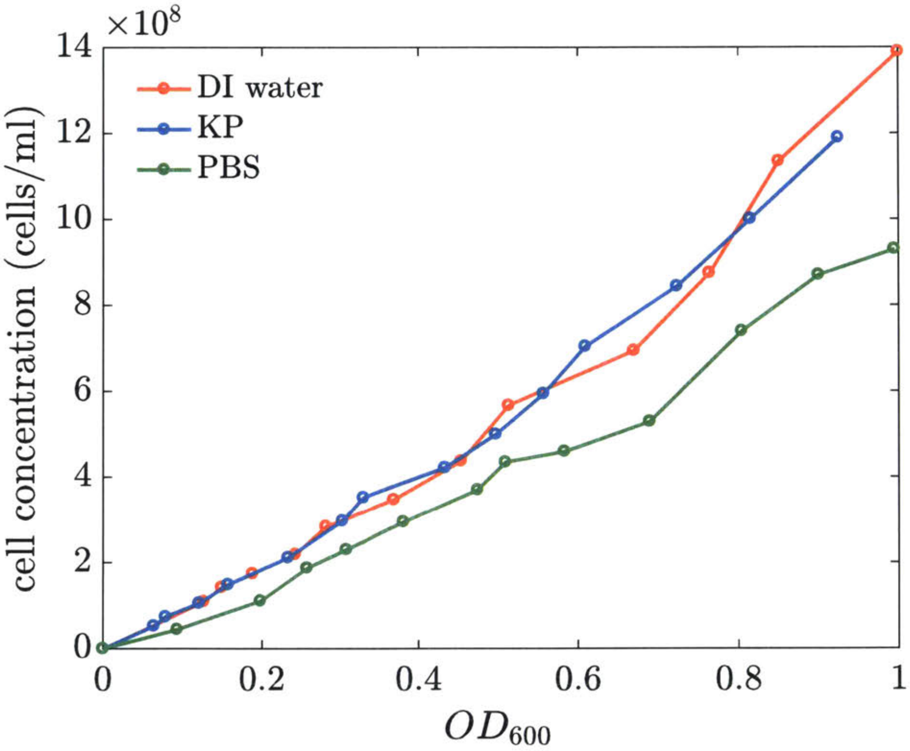

Figure 3-4: *E. coli* concentration as a function of the optical density at 600 nm (OD_{600}) in three different media: deionized (DI) water, and two other minimal solutions of salt: phosphate buffer (KP), and potassium phosphate buffer (PBS).

	time	High (H)	Middle (M)	Low (L)	Ultra Low (UL)	PBS	DI water
	0h	6.82	6.89	6.77	6.83	6.87	5.79
	0.5h	6.71	6.72	6.74	6.79	6.82	5.99
	1h	6.71	6.72	6.75	6.95	6.75	5.69
	1.5h	6.70	6.68	6.67	6.69	6.76	5.95
	2h	6.74	6.73	6.77	6.76	6.79	5.82
pH value	2.5h	6.74	6.73	6.77	6.76	6.79	5.52
	3h	6.67	6.68	6.70	6.70	6.72	5.89
	3.5h	6.59	6.51	6.69	6.58	6.71	6.10
	4h	6.58	6.72	6.76	6.62	6.69	5.71
	24h	6.71	6.78	6.75	6.72	6.82	5.76
	48h	6.74	6.72	6.73	6.76	6.76	5.96
	72h	6.78	6.76	6.74	6.79	6.82	5.52

Table 3.1: The pH evolution of *E.coli* with four different initial concentrations. The pH did not change a lot

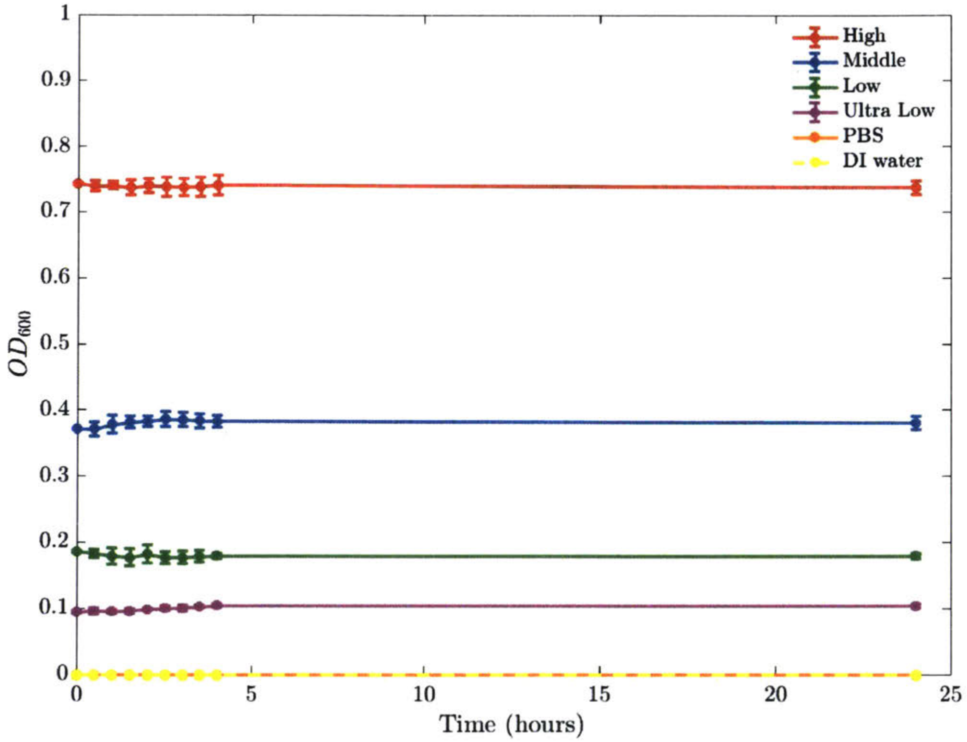

Figure 3-5: OD_{600} value of *E.coli* with five different initial concentrations. These time evolution show that *E. coli* in PBS do not grow, regardless of their initial concentration.

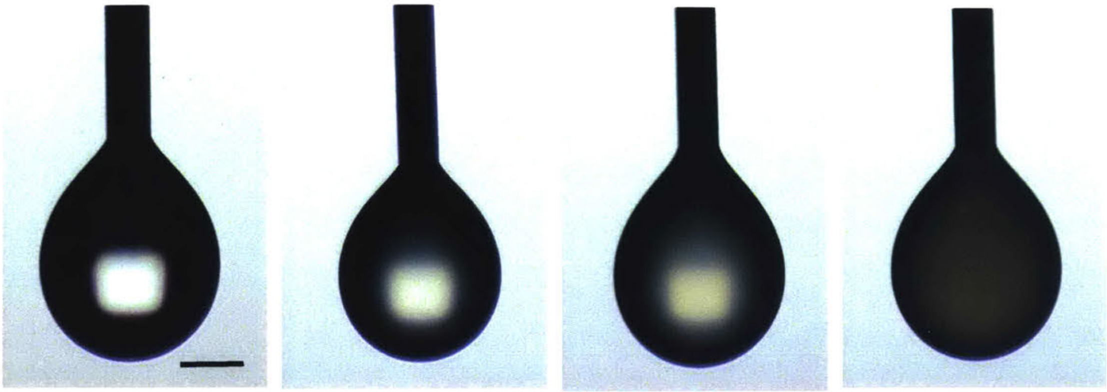

Figure 3-6: Bacteria phosphate buffer (KP) solution. From left to right, the concentration of bacteria increases, so that the transmittance of light decreases. However, surface tension changed little with concentration. Scale bar is 1 cm.

3.3.2 Surface tension

In addition, we also measure the surface tension of bacteria with different concentrations in two different minimal media to observe whether the concentration of bacteria will change the surface tension or not. We used tensiometer (Figure 3-6) to measure the surface tension by the pendant drop methods. A drop was produced by a needle, and then captured by camera. The drop profile is detected and can be used to find the value of the surface tension [80]

Figure. 3-7 shows the results of surface tension change with the concentration of bacteria in two different media. The result show that the surface tension did not change with bacteria concentration within the test range. This is important as we would like to test the contamination of bubbles in a manner that does not alter fundamentally their physics. Note however, that the effect of bacterial concentration could be subtle, involving dynamic rather than static surface tension changes. Indeed, clustering effects on the interface and increase of secretion of surfactant by such clusters of organisms could introduce small local gradients of surface tension, which can, in turn, drive distinct and rich surface dynamics on the bubble cap. Our focus in this thesis is to develop a method to visualize directly, quantify, and calibrate the particle or organism load in the bubble films. We shall discuss this further in the next chapter.

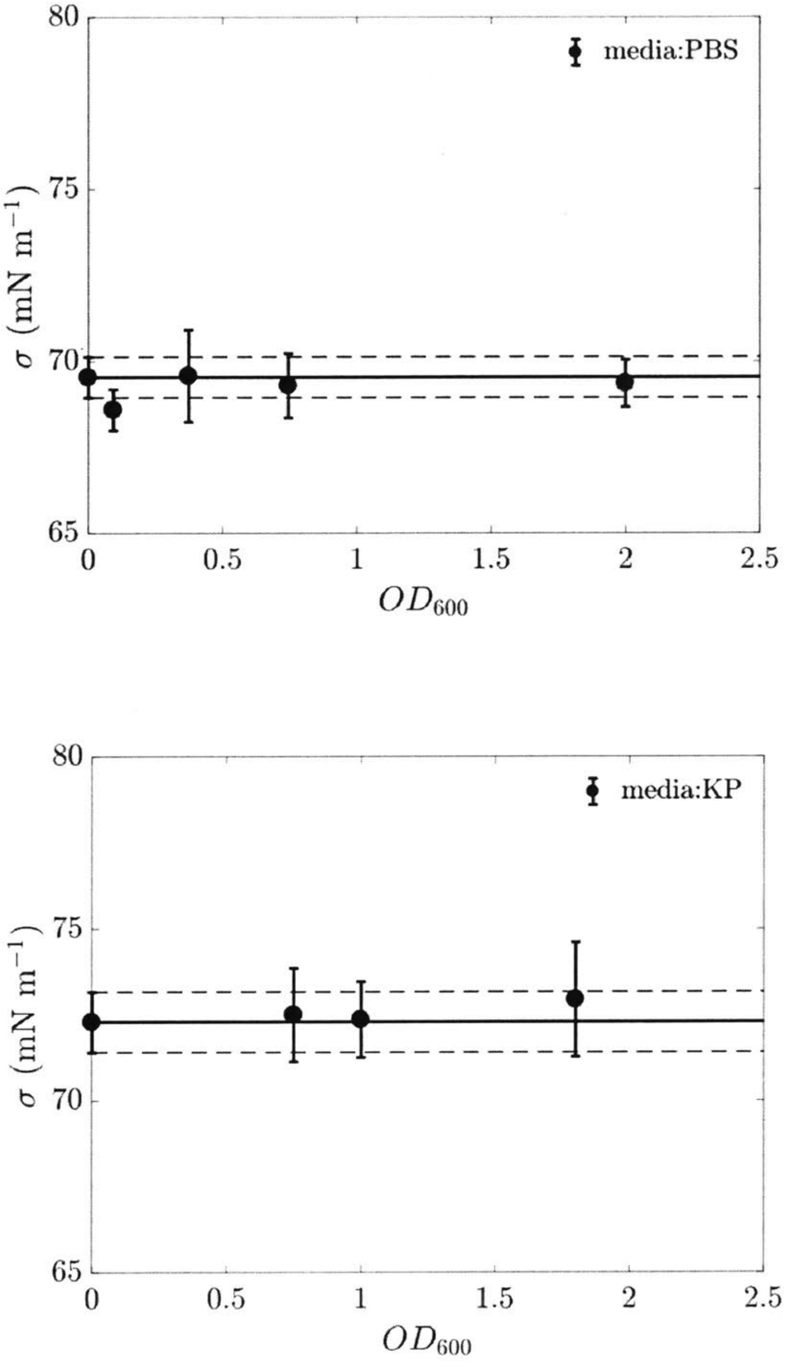

Figure 3-7: The surface tension of bacteria with different concentrations in different solutions. We can see that the concentration of bacteria will not change the surface tension of the solution in either PBS or KP.

Chapter 4

Schlieren imaging and design of the experiments

4.1 Introduction

As discussed in the first chapter, bubbles play essential roles in exchanging materials from water to the air. However, bubbles are small, and the particles inside bubbles are even smaller. Conventional imaging does not allow for visualization of particle movement on or in bubbles [81]. Due to this gap in direct visualization, the details of the interaction between small particles and bubbles remain speculative. To capture the fluid motion and particle movement in bubbles, we employed Schlieren imaging [81] to visualize inhomogeneities of the bubble cap. With this method, the number and movement of small particles such as bacteria and microspheres present in the bubble film can be readily observed. Using Schlieren imaging, we can observe black spots resulting from the presence of bacteria, but these spots are much larger than the bacteria themselves (Figure.4-1). The goal of this work is to calibrate the Schlieren spot size with the size of the original object. Indeed, we will see that the meniscus surrounding particles in the cap film shapes the Schlieren spot size observed. This is important from a fundamental point of view to understand contaminant-interface interactions in dynamic objects such as those of bubble caps. This is also important from a practical point of view to develop ways of tracking accurately the interaction

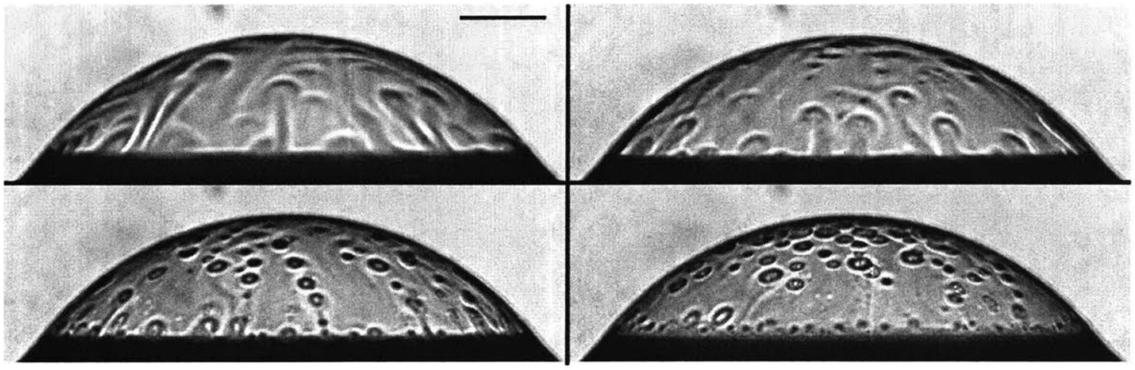

Figure 4-1: *E. coli* in a bubble film. The concentration of bacteria is approximately 5×10^8 cells/ml in DI water. The times are t =10, 26, 29, and 36s. The corresponding bubble cap thickness are h = 2.5, 1.3, 1.1, and 0.9 μm. Scale bar is 1mm. Reproduced from [1].

and changes in morphology and numbers of organisms or communities of organisms in situ on interfaces. This include, tracking cell division, interaction between organisms to study their predatory or cooperative dynamics and many more possibilities.

4.2 Bubble cap film thickness

The bubble cap film thickness controls the number, size, and speeds of droplets emitted at burst [43], therefore controlling the efficiency of the exchange of chemicals and pathogens from water to air (Chapter 1). Figure 4-2 shows an example of how we estimate the thickness of the bubbles at burst: we measure the speed of the hole nucleating on the bubble during its burst with precise image processing which is directly linked to the bubble thickness [82, 83]. In figure 4-3 we report our measurements of the thickness of bubble films as they burst after different lifetimes at the surface: older bubbles are thinner, they therefore generate smaller and faster droplets [43]. This also shows that the bubble cap film reaches a thickness of the order of 1 μm at long lifetimes, which is close to the size of the bacteria we study, *E. coli.* As we shall see in the next sections, this is why we are able to observe large Schlieren spots (Fig. 4-1 and 4-2) on old bubbles. We examine next how particles interact with films.

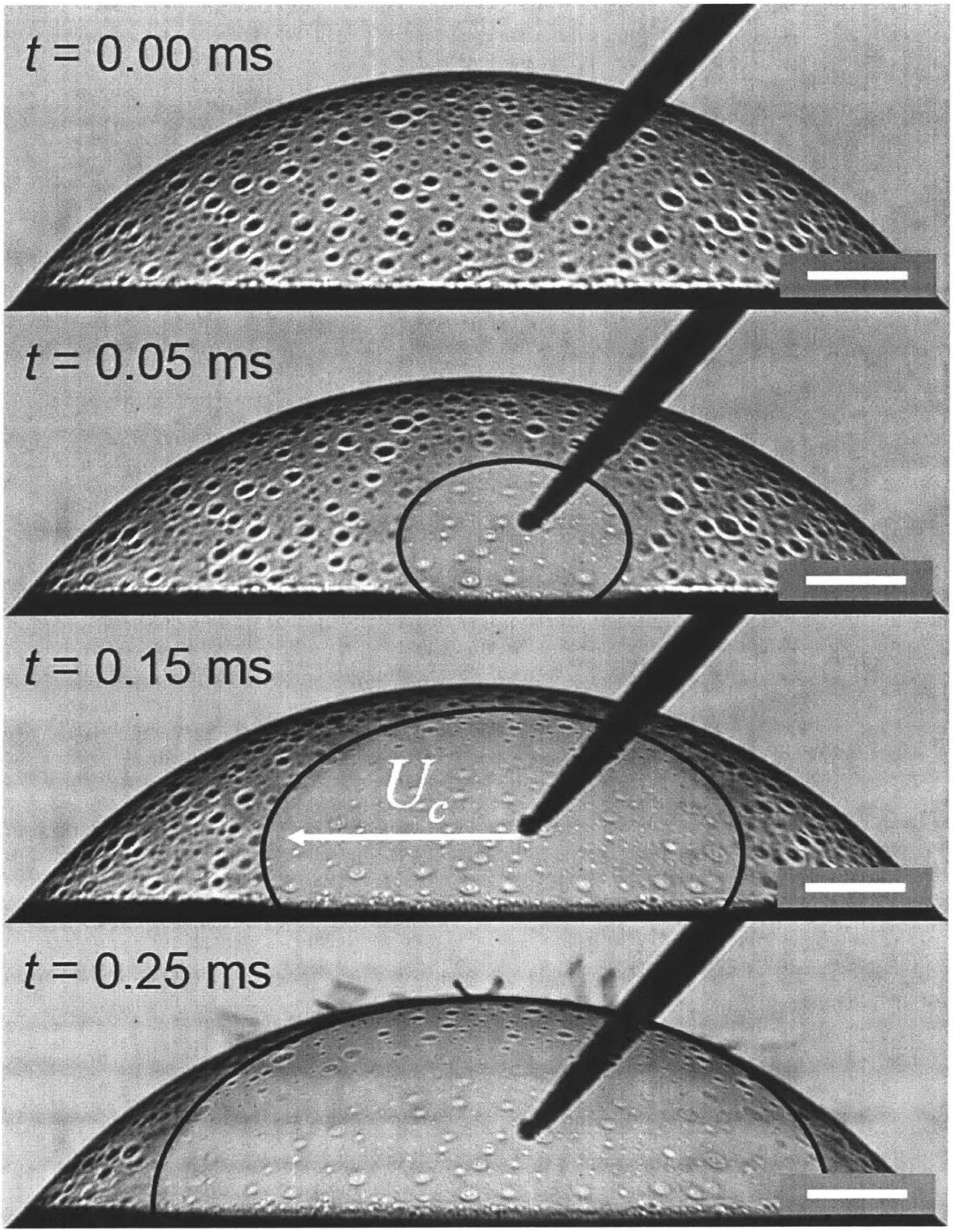

Figure 4-2: Measurement of the bubble cap film thickness. A needle punctures the film and creates a hole that recedes at constant speed U_c, related to the film thickness by Taylor-Culick relationship: $U_c = \sqrt{2\sigma/\rho h}$, where h is the film thickness, σ the surface tension and ρ is the density of fluid.

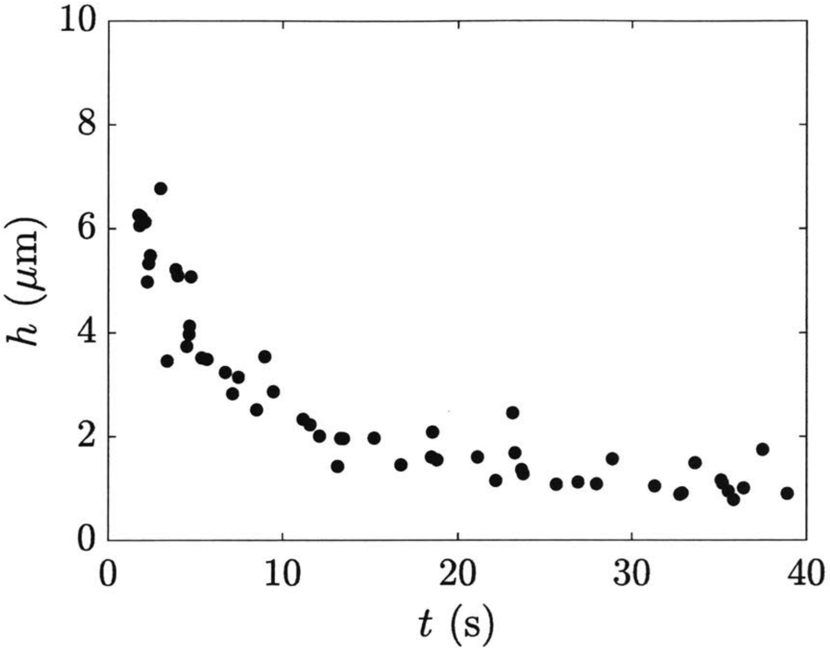

Figure 4-3: Bubble cap film thickness time evolution in deionized water inoculated with *E. coli* at $\mathrm{OD}_{600} = 0.474$. Each point correspond to a single bursting bubbles. The longer bubbles stay at the surface, the thinner they are.

4.3 Deformation of thin films

When a particle is present in a liquid film whose thickness is less than the particle diameter, a meniscus forms around the particle due the deformation of the fluid interface (Figure. 4-4). Danov et al. [9] derived the shape of this meniscus for a spherical particle. It is characterized by $z = \zeta(x, y)$ (Figure. 4-4) and follows Laplace equation:

$$\sigma\nabla \cdot \left[\frac{\nabla\zeta}{(1+|\nabla\zeta|^2)^{1/2}}\right] = P_c \tag{4.1}$$

where σ is the surface tension, P_c is the capillary pressure (the pressure difference across the meniscus), and ∇ is the two-dimensional gradient operator in the plane of the film. When the particle only slightly deforms the interface, the slopes are small ($\nabla\zeta \ll 1$) and equation (3.1) simplifies to:

$$\nabla^2\zeta = \frac{\zeta}{l_c^2} \tag{4.2}$$

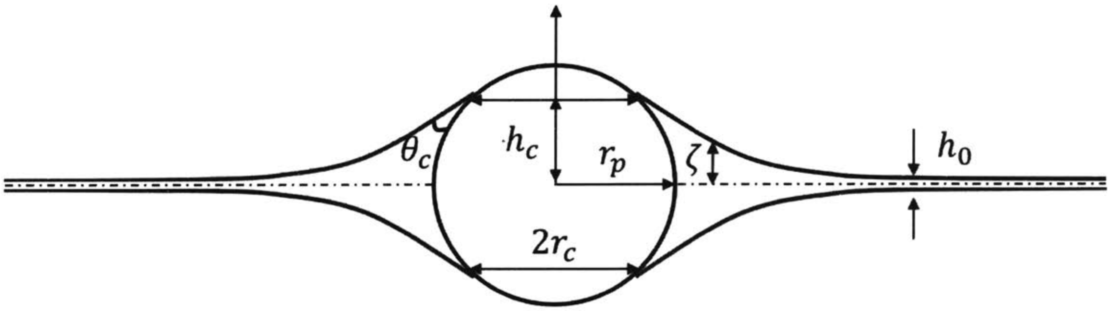

Figure 4-4: Particle entrapped in a thin liquid film of thickness h_0, which is smaller than the particle diameter $2r_p$. θ_c is the contact angle between the fluid in the film and the particles. Figure adapted from [9].

with

$$l_c = \sqrt{\frac{\sigma}{\rho g}} \tag{4.3}$$

the capillary length, the characteristic decay length of the interfacial deformation, ρ the water density and g is the acceleration due to gravity; This is a well know differential equation that can be solved to yield [9]:

$$\zeta(r) = AK_0\left(\frac{r}{l_c}\right) \tag{4.4}$$

where r is the radial distance from the particle center, K_0 is the modified zero order Bessel function of second kind, and A is a constant of integration that depends on the film thickness, particle radius, particle wetting properties. We shall determine the relationship between these three variables next.

4.4 Schlieren visualization

4.4.1 Bacteria and particles in bubbles

When bacteria are present in a thin bubble film they can deform it as explained above. Figure 4-1 shows *E. coli* revealed in a bubble cap film with Schlieren imaging. *E.coli* are typically rod shaped, about 2.0 μm in length and 0.25 to 1 μm in diameter. In this figure, it is clear that we are not able to visualize *E. coli* when the bubble cap is

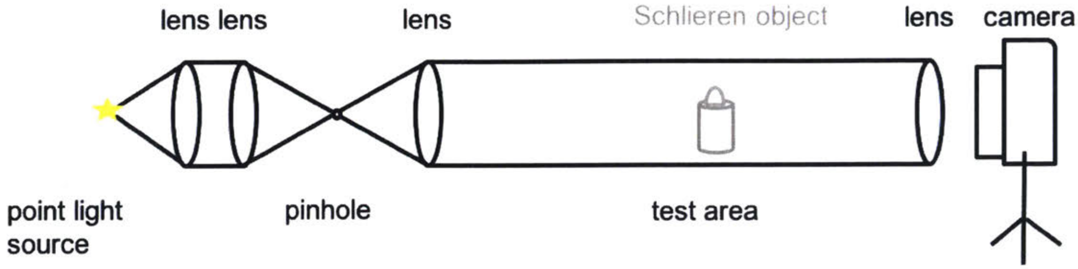

Figure 4-5: Diagram of a Schlieren setup. Rays from an initial light sources go through 3 lenses and a pinhole to generate parallel beams. In the test area, light is deflected when it encounters a change of optical index, such as when going through a bubble. The beam are then refocused on the sensor of a camera.

too thick. However, when it lives long enough to reach thicknesses that are less than approximately 1.5 μm, the typical the length of *E.coli*, large dark spots are observed. They originate from the meniscus profile derived in the previous section.

Light propagates uniformly in homogeneous media, but when a parallel beam travels through a region of nonuniform density, or of distinct refractive index, it is deflected. Schlieren imaging takes advantage of this property to reveal such density variations [81, 84]. Here, we use it to visualize variations of thicknesses in the caps of bubbles. We set up a Schlieren system with a point light source, a pinhole, four lenses, and a camera (Figure.4-5) and used it to visualize bubbles (e.g., Fig. 4-1 and 4-2). To verify that what we observe with bacteria on bubbles in Figure 4-1 is consistent with the meniscus profile derived in 4.3, a ray-tracing algorithm was developed to simulate Schlieren images of such menisci. This is illustrated Figure 4-6($a-c$): parallel light arrives perpendicular to a thin film which contain a particle that deforms the film according to Eq.(4.4). Our optical experimental setup is then simulated to obtain a numerical estimation of what would be observed on our camera. Clearly, the film thickness plays an important role also in the spot size, hence the importance of measuring it directly as well for this calibration of spot to particle size. Recall that we can measure film thickness as shown in figure 4-2.

The simulated images are very similar to what we observe when we seed bubbles with bacteria (Fig.4-1) particles of different sizes (Figure 4-6(d)).

We just demonstrated that quantitative information on bacteria or particles present

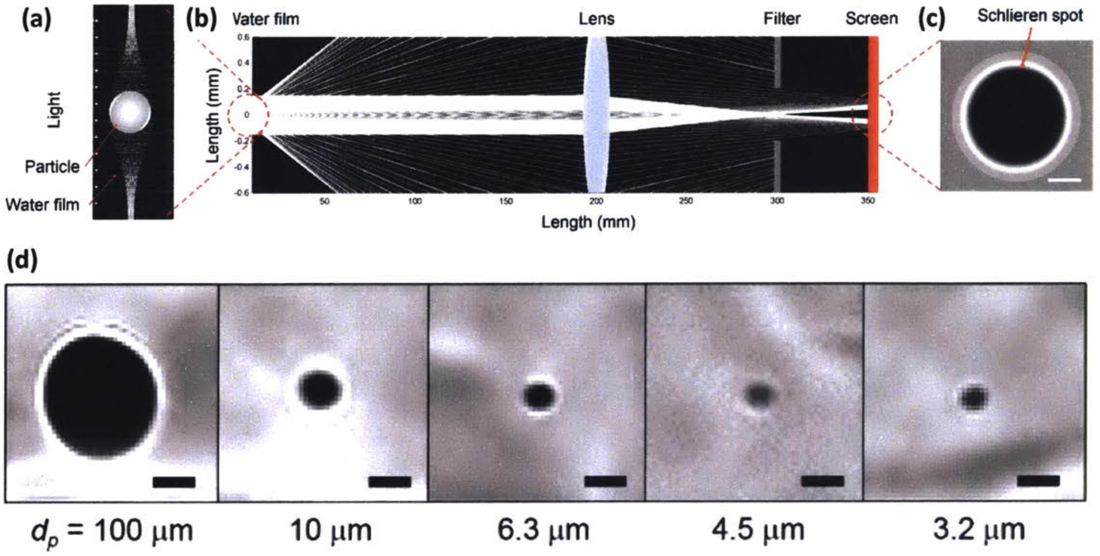
(a)
Light
Particle
Water film
(b)
Vater film
Lens
Filter
Screen
Length (mm)
0.6
0.4
0.2
0
-0.2
-0.4
-0.6
50
100
150
200
250
300
350
Length (mm)
(c)
Schlieren spot
(d)
d_p = 100 μm
10 μm
6.3 μm
4.5 μm
3.2 μm

Figure 4-6: Numerical Schlieren visualization of a meniscus around a particle in a thin film (*a*). After parallel light goes through the meniscus, the Schlieren optical setup (*b*) acts as a magnifier: the trace of the particle on the camera sensor (*c*) is larger than the particle itself. Schlieren images of menisci from experiments (*d*) show a very good agreement with the simulation (Scale bars: 100 μm).

in bubble films can be obtained from Schlieren. However, obtaining precise data with bacteria and on bubbles is very challenging. First, the thickness of bubbles changes with the age of the bubble (Figure 4-3). Second, the size of the meniscus profile is also difficult to measure due to the continuous movements of the bubble at the surface and to its curvature.

To gain insights and obtain a calibration between the spot and particle sizes, we move on to an analog system: particles in a flat soap film. The advantage is the control of particle size and shape and the more precise evolution of its film thickness.

4.4.2 Particles in flat films

The thickness gradients of a soap film can be observed by interference fringes color matching [85], which results in more precise measurements than an estimation of the Taylor-Culick speed on bubbles (Fig. 4-3). We also use commercial spherical particles of known diameter and geometry.

Figure 4-7 shows Schlieren images of particles on a flat films, where Schlieren spots

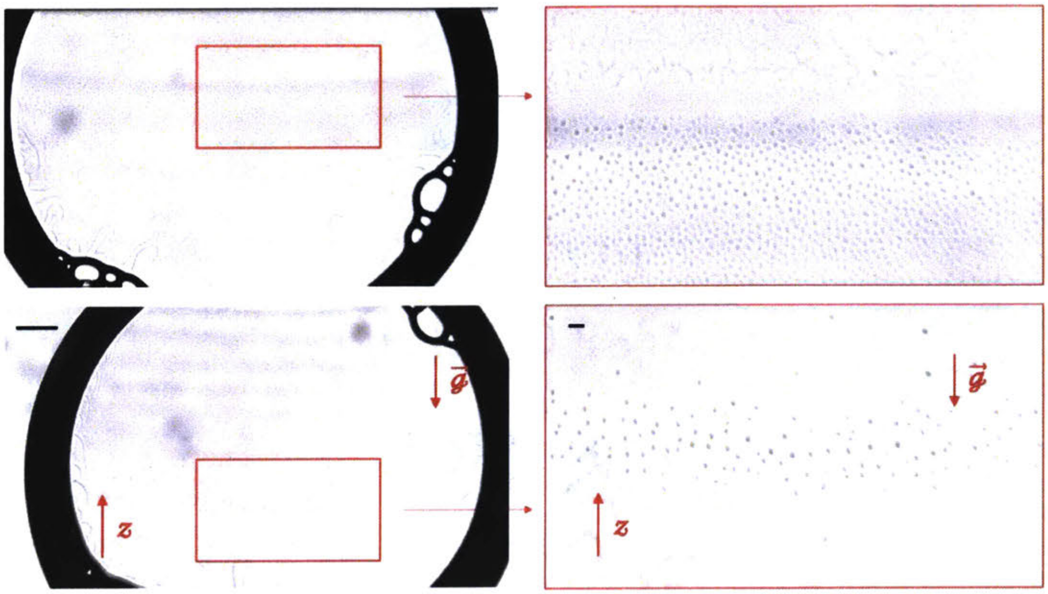

Figure 4-7: Particles in a flat soap film. The upper one is particle with diameter = 0.5 μm, the lower one is particle with diameter = 2 μm. Scale bar is 1 cm. g is the direction of gravity.

are also clearly identified. A soap film drains due to gravitational drainage, and its upper part is therefore thinner than its lower part. This explains why we are able to observe 0.5 μm particles at the top of the soap film, but only 2 μm particles at the bottom when using two different sizes of particles.

4.4.3 Rods in bubbles

The experiments described previously show that when the film thickness is close to the size of the perturbation, the micrometric particles or bacteria can be observed with regular Schlieren imaging. However, the precise relationship between the spot size, particle size, and wetting properties of the particle are experimentally challenging.

A first simplifying assumption consists in neglecting the influence of the film thickness. To do so, we pierce bubbles (Fig. 4-8) or flat soap films (Fig. 4-10) with cylindrical rods much larger (50 to 100 times) than the film thickness. Figure 4-8 shows a bubble with a rod through it: a Schlieren spot, much larger than the rod

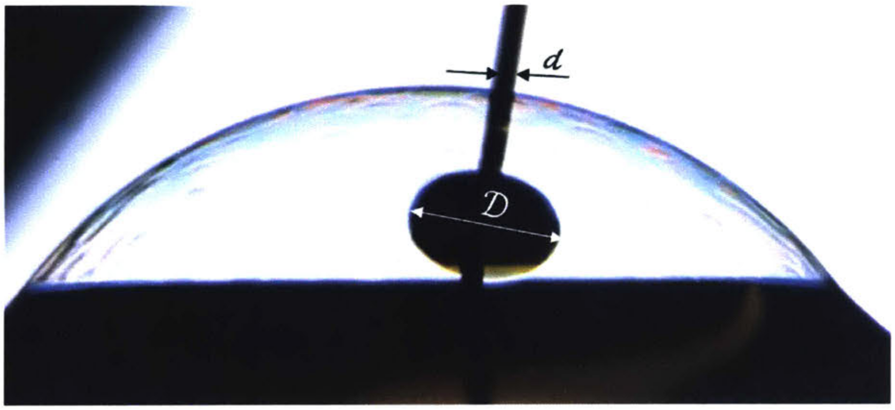

Figure 4-8: Copper rod going through a bubble. We can observe a meniscus profile around it. d is the diameter of the rod, D is the diameter of the meniscus profile. $d = 260\mu\text{m}$, $D = 2.33$ mm.

diameter (by a factor ten here), is also observed. While these experiments with rods and bubbles were promising, they are also challenging since bubbles still move while at surface, and also because pinning the cylinder in the bubble film at the right angle in a systematic manner is difficult. Figure. 4-9 shows the results of Schlieren radius ($R_{meniscus}$) of steel rods with different diameters as a function of time. We can see that the results have too much noise. In order to study the different parameters one by one, we next study rods in flat soap films.

4.4.4 Rods in flat films

With flat films we are able to guarantee that the rod always penetrate the film normal to its surface. Figure 4-10 shows the experimental setup. The results are presented in the next chapter.

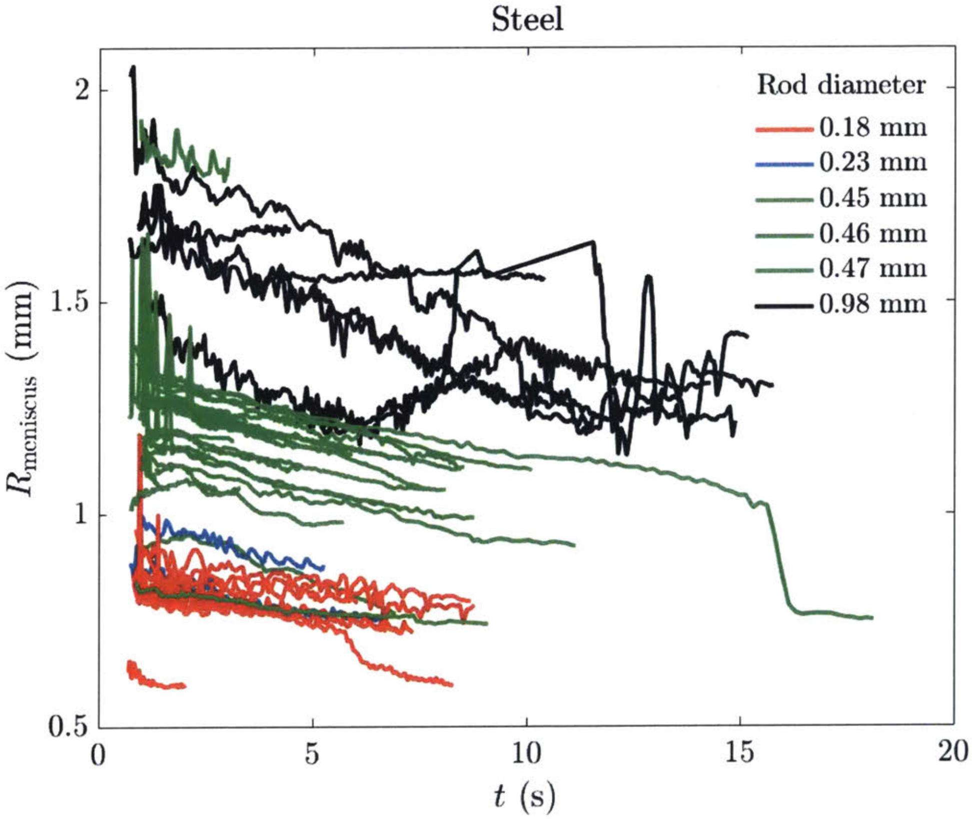

Figure 4-9: Schlieren radius ($R_{meniscus}$) of steel rods with different diameters as a function of time.

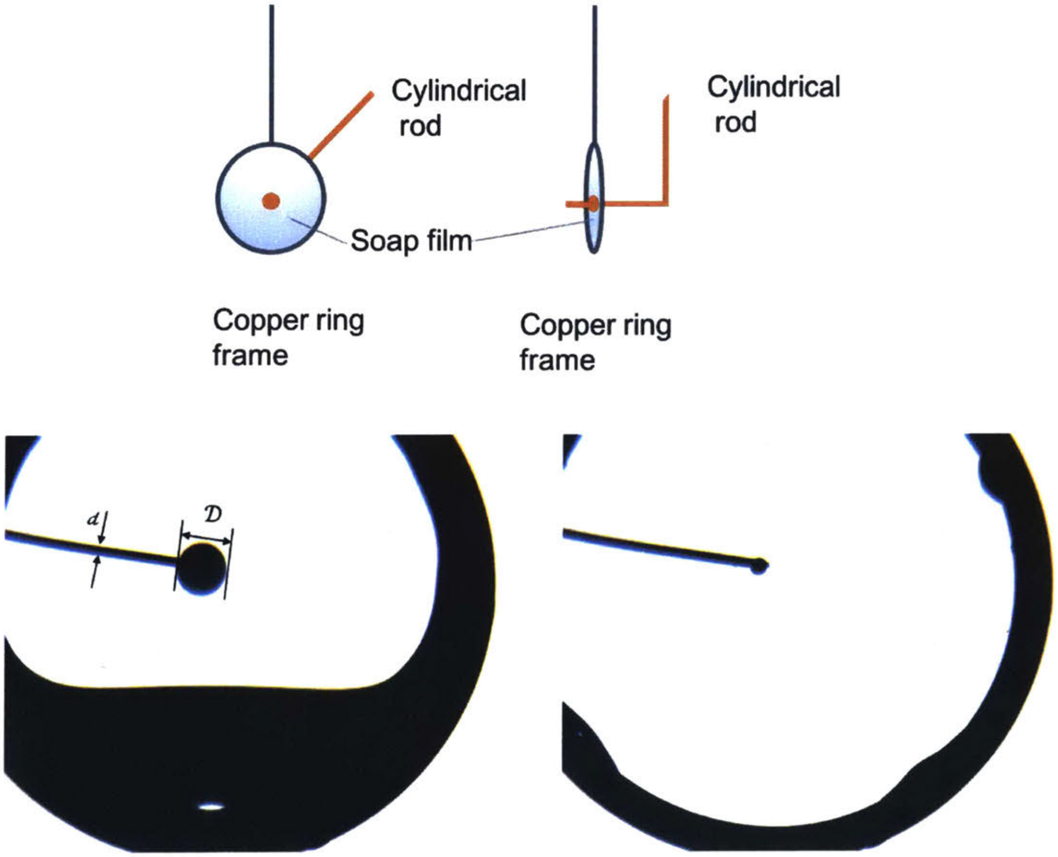
Cylindrical rod
Soap film
Copper ring frame
Cylindrical rod
Copper ring frame
d
D

Figure 4-10: When a cylindrical needle is placed in a soap film, we can observe a meniscus profile around it (left down). After the film bursts, the meniscus profile disappears (right down). d is the diameter of the rod, D is the diameter of the meniscus profile. $d = 137\mu$m, $D = 1.87mm$.

Chapter 5

Schlieren visualization: spot size to particle size ratio

The previous chapter described the effect of bacteria on bubbles: when the cap film becomes thin enough, bacteria are revealed macroscopically using Schlieren imaging. Obtaining quantitative information from such visualization is challenging, and we describe the simplest analogue experiments allowing us to gain insights on this technique: a cylindrical rod pinned into a flat soap film.

Our experimental setup is represented Fig. 5-1: a circular soap film is created by dipping a copper ring into a soap solution. We used cylindrical rods with different materials (yellow copper, white copper, steel, and nickel) and diameters (from 50 to 1000 μm, precisely measured with a microscope as shown in figure 5-2). Because we expect the wetting properties to be important, we measured the contact angle of each rod by dipping them in a reservoir of solution with the same composition as the one used to dip copper ring (Figure. 5-3) but found little variation (it ranges from 15 to 50 ° for all rods studied herein). We then compare our experimental data with the Schlieren simulations described in Section 4.4 (Fig. 4-6).

We create soap films with a solution of deionized water and sodium dodecyl sulfate (SDS), with a concentration of 0.3 cmc (critical micelle concentration). SDS is a common industrial surfactant, and we chose the lowest concentration that allows to maintain the soap film when it is pierced by a rod. Indeed, we want to stay as close

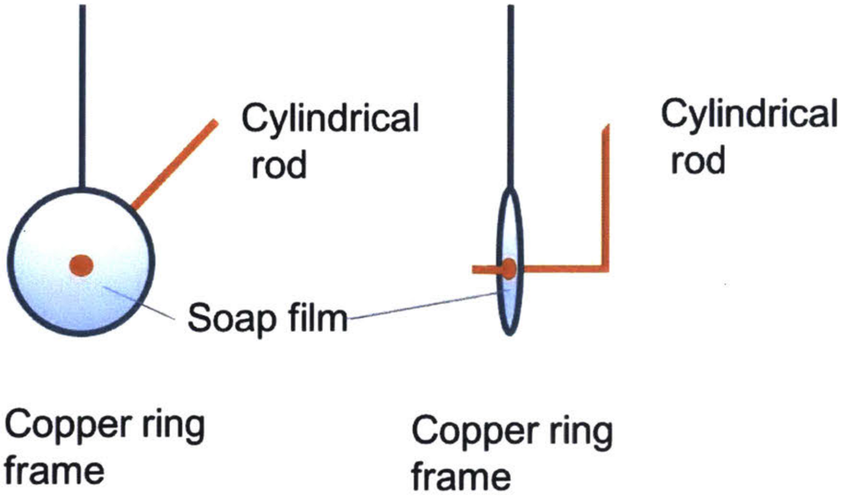
Cylindrical rod
Cylindrical rod
Soap film
Copper ring frame
Copper ring frame

Figure 5-1: The set up of the Copper Ring frame. We used 1mm diameter copper wire to make the ring frame.

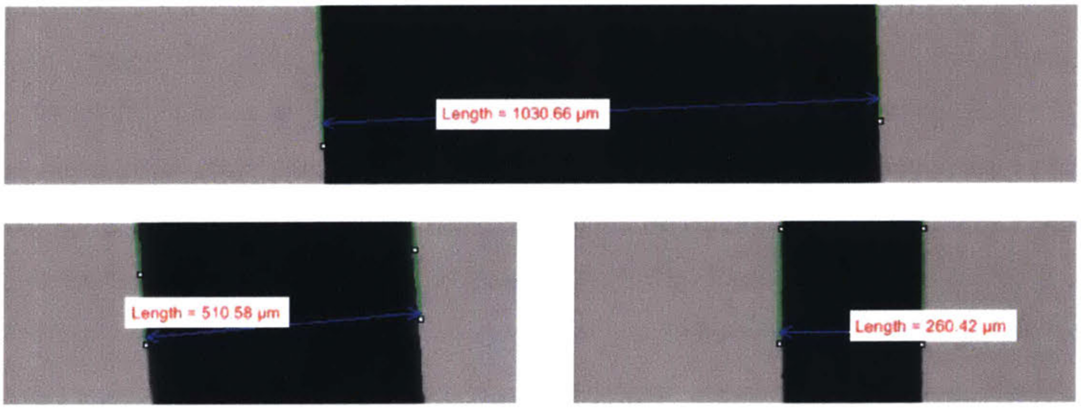
Length = 1030.66 μm
Length = 510.58 μm
Length = 260.42 μm

Figure 5-2: The diameter of yellow copper rods were measured under the microscope.

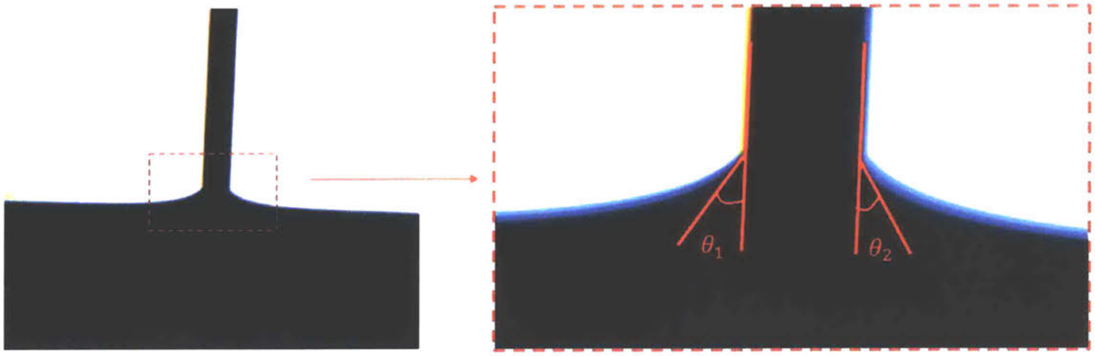

Figure 5-3: Contact angle measurement. θ_1 and θ_2 are the two contact angles, measured using a in-house precise image processing code

as possible to water for our results to apply for bubbles as well.

5.1 Results and summary

Our experimental results are presented in Figure 5-4 along with the results of the simulations. In both cases, variations for different material and hence different contact angles are small, showing that the wetting properties do not seem to affect the Schlieren spot size, at least in the limit case where the perturbation is much larger than the film thickness. While our simulations capture the trends observed in the experimental data, there is also a systematic offset between the two. A better understanding of the discrepancy between the theoretical meniscus profile derived in 4.3 (Chapter 4) used in our computation will be the focus of future work.

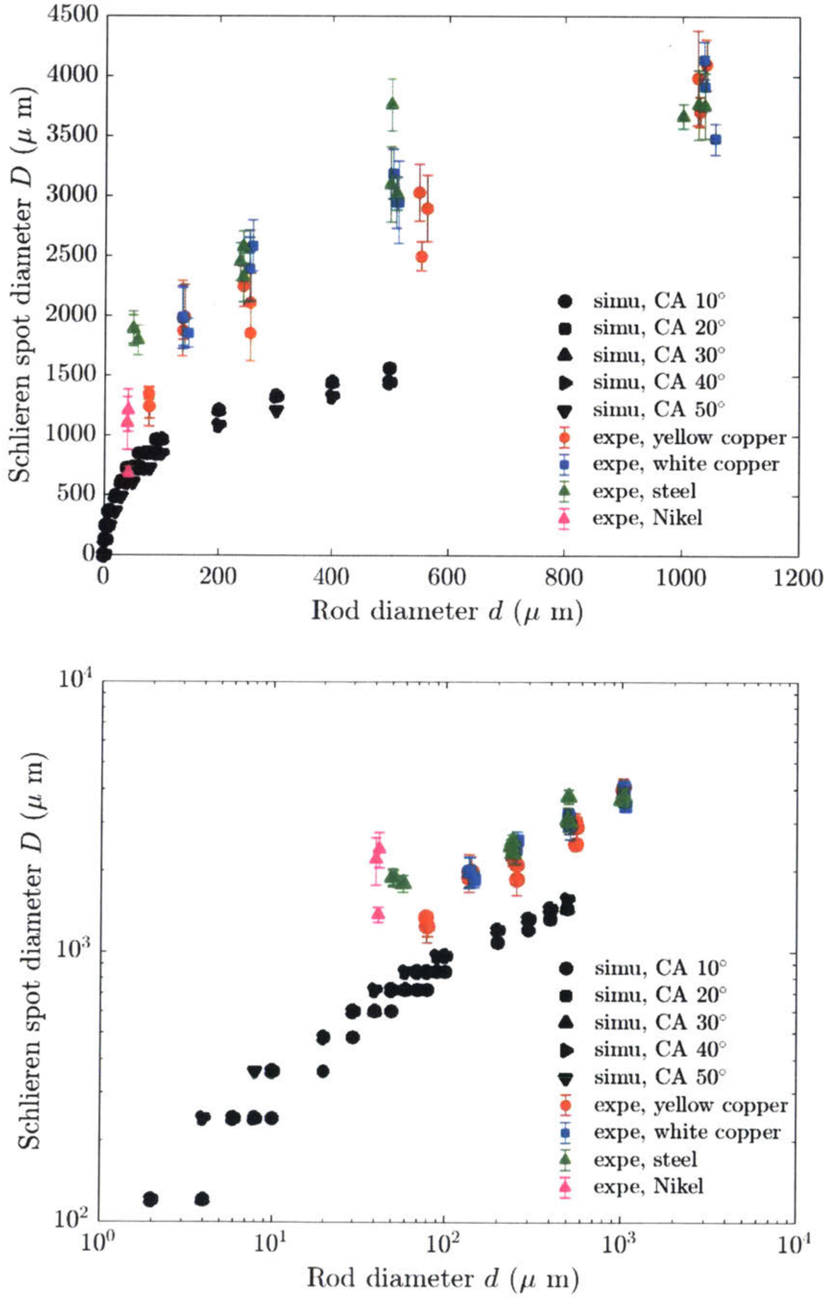

Figure 5-4: Schlieren spot diameter as a function of the rod diameter. Results from experiments (colors) and simulations (black) are represented. CA refers to contact angle.

Chapter 6

Discussion and conclusion

Bubble bursts are among the most efficient and ubiquitous producers of sea spray and contaminated droplets indoors. They contribute to the dispersal of organic, inorganic, and biological compounds in the air we breath and change the atmospheric physics and heat exchange while also changing the surf zone ecosystems inland. What sets the concentration of organisms of chemicals or particles in the droplets they produce remain unknown. Although the dynamics of scavenging of biological or chemical agents during the rise of the bubble can play a role, another mechanism of interaction of the bubble with the bulk after surfacing could also play a key role. This latter mechanism has been neglected so far. One major hurdle to overcome is the methodology that would allow to study such dynamics systematically. So far, this has been lacking. In this thesis, we focused on addressing this gap and challenge by developing a method for the visualization of contaminated bubble caps after they surface. We aimed to develop a method that can quantify directly the dynamics of interaction between the contaminants, particles or organisms, and the thin film they are trapped in.

In the first part, we showed that an optical technique relying on visualization method called Schlieren or Shadowgraphy imaging could allow to reveal inclusions in bubble films. We then moved on to prepare a range of inclusions from particles to bacterial organisms and test for the ability of the method to reveal both. We showed that the organisms and particles are revealed in the form of spots when the size of the film they are trapped in become comparable to that of the size of the particle or bacteria.

We then moved on to develop a more quantitative calibration method to link directly the spot size that our method allow to reveal on the bubble or thin film and the original size of the particle or bacteria within the film. This was done with a range of systematic experiments that controlled the particle sizes and quantified the film thicknesses involved. We also used a calibration method using analog experiments using flat films rather than curved bubble films for ease of measurement.

The analog experiments and measurements allowed to develop a theoretical model explaining the spot sizes revealed by our method, using ray-tracing optical methods (Chapter 4). We validated this method with a range of particles and rods of a range of wetting properties and sizes. We recovered the trend observed. In particular, we showed that when the the diameter of an inclusion such as a rod is much larger than the film thickness (larger than 150 μm for example), the radii of meniscus profiles generated by different materials with different contact angles but similar radius are very close to each other. However, when the rod diameter is small (less than 150 μm for example), the radii of meniscus profiles generated by different materials with similar radii can vary significantly.

Finally, returning to the biological contamination of films, our results showed that the Schlieren spot sizes of biological contaminants in bubbles can be matched to their actual size via our calibration to the first order. Indeed, while our ray-tracing model captures the trends observed in the experimental data, there is also a systematic offset between the two. A better understanding of the discrepancy between the theoretical meniscus profile derived in 4.3 (Chapter 4) used in our computation will be the focus of future work to refine further this methodology. This last refinement step will be important if one needs a more precise calibration to track organism sizes as they evolve and divide, cluster or to understand the interaction between communities of organisms in thin interfaces.

In sum, this project focused on the development of a novel technique to study contaminated interfaces. We focused on development and calibration of the method.

This method can have important applications in fundamental research, for example for understanding the physics and biology of enrichment of bubbles and water-to-air transfer of contaminants. The latter is critical for the transport of biological, chemical, or particulate contaminants shaping disease transmission, chemical spills, climate, ecology, and bio-hazard risks. Moreover, this method can also have important applications as a technology that can be used to study large scale interactions of bacterial or organismic communities in thin films in a manner not allowed at this stage by regular microscopy.

Bibliography

[1] S. Poulain, E. Villermaux, and L. Bourouiba. Ageing and burst of surface bubbles. *Under review*, 2018.

[2] L. Bourouiba, E. Dehandschoewercker, and J. W. M. Bush. Violent expiratory events: on coughing and sneezing. *J. Fluid. Mech.*, 745:537âĂŞ563, 2014. doi: 10.1017/jfm.2014.88.

[3] L. Bourouiba. A sneeze. *N. Engl. J. Med.*, 375(8):e15, 2016.

[4] Laken S. Lu C.-C. Maa R. Langer R. Traverso, G. and L. Bourouiba. Fluid fragmentation from hospital toilets. arXiv:1310.5511, 2013.

[5] P. L. L. Walls, J. C. Bird, and L. Bourouiba. Moving with bubbles: A review of the interactions between bubbles and the microorganisms that surround them. *Integrative and comparative biology*, 54(6):1014–1025, 2014.

[6] F. Veron. Ocean spray. *Annual Review of Fluid Mechanics*, 47 (1):507–538, 2015. ISSN 0066-4189-1545-4479. doi: 10.1146/annurev-fluid-010814-014651. URL `http://annualreviews.org/doi/abs/10.1146/annurev-fluid-010814-014651`.

[7] M. Cunliffe and J.C. Murrell. The sea-surface microlayer is a gelatinous biofilm. *The ISME journal*, 3(9):1001–1003, 2009. doi: 10.1038/.

[8] P. L. L. Walls, J. C. Bird, and L Bourouiba. Moving with bubbles: A review of the interactions between bubbles and the microorganisms that surround them. *Integr. Comp. Biol.*, 54(6):1014–1025, 2014.

[9] K. D. Danov, B. Pouligny, and P. A. Kralchevsky. Capillary forces between colloidal particles confined in a liquid film: The finite-meniscus problem. *Langmuir*, 17(21):6599–6609, 2001.

[10] G.S. Settles. Fluid mechanics and homeland security. *Annu. Rev. Fluid Mech.*, 38:87–110, 2006.

[11] J. W. Tang, Y. Li, I. Eames, and G.L. Chan, P.K.S.and Ridgway. Factors involved in the aerosol transmission of infection and control of ventilation in healthcare premises. *J. Hosp. Infect.*, 64(2):100 – 114, 2006. ISSN 0195-6701.

[12] Staples S. Dabiri J.-Marsden A. Prakash M. Davis K. Shadden S. Savin T. Bourouiba L. Sznitman J. Jung, S. Research trends in biological fluid dynamics. *Research Trends in Biological Fluid Dynamics. US National Committee on Theoretical and Applied Mechanics (USN/TAM) Invited Report on Recent Trends in Mechanics. Publications of the US National Academies of Sciences, Engineering, and Medicine.*, 2016.

[13] S. Zhu, S. Kato, and J. Yang. Study on transport characteristics of saliva droplets produced by coughing in a calm indoor environment. *Building and Environment*, 41(12):1691 – 1702, 2006.

[14] I. Eames, J. W. Tang, Y. Li, and P. Wilson. Airborne transmission of disease in hospitals. *J. R. Soc. Interface.*, 2009. ISSN 1742-5689. doi: 10.1098/rsif.2009.0407.focus.

[15] D. C. Blanchard. The ejection of drops from the sea and their enrichment with bacteria and other materials: A review. *Estuaries*, 12(3):127–137, Sep 1989. ISSN 0160-8347.

[16] K.F. Fannin, S.C. Vana, and W. Jakubowski. Effect of an activated sludge wastewater treatment plant on ambient air densities of aerosols containing bacteria and viruses. *Appl. Environ. Microbiol.*, 49(5):1191–1196, 1985.

[17] H. Bauer, M. Fuerhacker, F. Zibuschka, H. Schmid, and H. Puxbaum. Bacteria and fungi in aerosols generated by two different types of wastewater treatment plants. *Water Res.*, 36(16):3965 – 3970, 2002.

[18] Stephen KC Ng. Possible role of an animal vector in the sars outbreak at amoy gardens. *Lancet*, 362(9383):570 – 572, 2003. ISSN 0140-6736.

[19] J. O. Falkinham III. Mycobacterial aerosols and respiratory disease. *Emerg. Infect. Diseases*, 9(7):763, 2003.

[20] J. Embil, P. Warren, M. Yakrus, R. Stark, S. Corne, D. Forrest, and E. Hershfield. Pulmonary illness associated with exposure to mycobacterium-avium complex in hot tub water: Hypersensitivity pneumonitis or infection? *Chest*, 111(3):813 – 816, 1997.

[21] Theodore W. Wilson, Luis A. Ladino, Peter A. Alpert, Mark N. Breckels, Ian M. Brooks, Jo Browse, Susannah M. Burrows, Kenneth S. Carslaw, J. Alex Huffman, Christopher Judd, Wendy P. Kilthau, Ryan H. Mason, Gordon McFiggans, Lisa A. Miller, Juan J. Nájera, Elena Polishchuk, Stuart Rae, Corinne L. Schiller, Meng Si, Jesús Vergara Temprado, Thomas F. Whale, Jenny P. S. Wong, Oliver Wurl, Jacqueline D. Yakobi-Hancock, Jonathan P. D. Abbatt, Josephine Y. Aller, Allan K. Bertram, Daniel A. Knopf, and Benjamin J. Murray. A marine biogenic source of atmospheric ice-nucleating particles. *Nature*, 525(7568):234–238, 2015. ISSN 0028-0836. doi: 10.1038/nature14986.

[22] H. Agogue, E. O. Casamayor, M. Bourrain, I. Obernosterer, F. Joux, G. J. Herndl, and P. Lebaron. A survey on bacteria inhabiting the sea surface microlayer of coastal ecosystems. *FEMS Microbiol Ecol*, 54(2):269–80, 2005. ISSN 0168-6496 (Print)0168-6496 (Linking). doi: 10.1016/j.femsec.2005.04.002. URL `https://www.ncbi.nlm.nih.gov/pubmed/16332325`.

[23] J. Y. Aller, M. R. Kuznetsova, C. J. Jahns, and P. F. Kemp. The sea surface microlayer as a source of viral and bacterial enrichment in marine aerosols. *J. Aerosol Sci.*, 36(5):801–812, 2005. ISSN 0021-8502. doi: http://dx.doi.org/10.1016/j.jaerosci.2004.10.012.

[24] A. Cunliffe, M.and Engel, S. Frka, B. GaâĽĹÂřparoviÆŠÂą, C. Guitart, J. C. Murrell, M. Salter, C. Stolle, R. Upstill-Goddard, and O. Wurl. Sea surface microlayers: A unified physicochemical and biological perspective of the airâĂŽÃĎÃňocean interface. *Progress in Oceanography*, 109:104–116, 2013. ISSN 00796611. doi: 10.1016/j.pocean.2012.08.004. URL `http://www.sciencedirect.com/science/article/pii/S0079661112000924`.

[25] M. Cunliffe, R. C. Upstill-Goddard, and J. C. Murrell. Microbiology of aquatic surface microlayers. *FEMS Microbiol Rev*, 35(2):233–46, 2011. ISSN 1574-6976-0168-6445. doi: 10.1111/j.1574-6976.2010.00246.x. URL `https://www.ncbi.nlm.nih.gov/pubmed/20726895`.

[26] A. Engel and L. Galgani. The organic sea surface microlayer in the upwelling region off peru and implications for airâĂŽÃĎÃňsea exchange processes. *Biogeosciences Discussions*, 12(13):10579–10619, 2015. ISSN 1810-6285. doi: 10.5194/bgd-12-10579-2015. URL `http://citeseerx.ist.psu.edu/viewdoc/download?doi=10.1.1.737.4227&rep=rep1&type=pdf`.

[27] I. Obernosterer, Philippe C., Lami R., Jocelyne C., Josephine R., Anncik Br., Claire D., France V. W., and Philippe L. Biochemical characteristics and bacterial community structure of the sea surface microlayer in the south pacific ocean. *Biogeosciences*, 5(3):693–705, 2008. URL `http://hal.upmc.fr/hal-00330708/`.

[28] W. Tianzhi, L. Yunkai, L. Mingchao, Y. Peiling, and B. Zhihui. Biofilms on the surface of gravels and aquatic plants in rivers and lakes with reusing reclaimed water. *Environmental Earth Sciences*, 72(3):743–755, 2013. ISSN 1866-6280-1866-6299. doi: 10.1007/s12665-013-2998-3. URL `http://link.springer.com/article/10.1007/s12665-013-2998-3`.

[29] M. Wurl, O.and Holmes. The gelatinous nature of the sea-surface microlayer. *Marine Chemistry*, 110(1-2):89–97, 2008. ISSN 03044203. doi: 10.1016/j.marchem.2008.02.009. URL `http://www.sciencedirect.com/science/article/pii/S0304420308000303`.

[30] M. Gade, H. HâĽŽÂžhnerfuss, and G. Korenowski. *Marine surface films*. Springer, 2006.

[31] D. Rosenfeld, R. Lahav, A. Khain, and M. Pinsky. The role of sea spray in cleansing air pollution over ocean via cloud processes. *Science*, 297(5587), 2002. URL `http://science.sciencemag.org/content/297/5587/1667`.

[32] R. E. Baier. Organic films on natural waters: Their retrieval, identification, and modes of elimination. *Journal of Geophysical Research*, 77(27):5062–5075, 1972. ISSN 01480227. doi: 10.1029/JC077i027p05062. URL `http://onlinelibrary.wiley.com/doi/10.1029/JC077i027p05062/full`.

[33] D. C. Blanchard and Lawrence Syzdek. Mechanism for the water-to-air transfer and concentration of bacteria. *Science*, 170(3958):626–628, 1970. doi: 10.1126/science.170.3958.626.

[34] S. A. Crow, D. G. Ahearn, W. L. Cook, and A. W. Bourquin. Densities of bacteria and fungi in coastal surface films as determined by a membrane-adsorption procedure1,2. *Limnology and Oceanography*, 20(4):644–646, 1975. ISSN 1939-5590.

[35] T. M. Preston. The water-air interface: a microhabitat for amoebae. *European Journal of Protistology*, 39(4):385–389, 2003. ISSN 09324739. doi: 10.1078/0932-4739-00008. URL `http://www.sciencedirect.com/science/article/pii/S0932473904701145`.

[36] R.S. Wotton. Does the surface film of lakes provide a source of food for animals living in lake outlets? *Limnology and Oceanography*, 27(5):959–960, 1982. URL `http://onlinelibrary.wiley.com/doi/10.4319/lo.1982.27.5.0959/full`.

[37] J-H Liang, J. C. McWilliams, P. P. Sullivan, and B. Baschek. Modeling bubbles and dissolved gases in the ocean. *Journal of Geophysical Research*, 116(C3), 2011. ISSN 0148-0227. doi: 10.1029/2010jc006579. URL `http://onlinelibrary.wiley.com/doi/10.1029/2010JC006579/full`.

[38] J-H Liang, J. C. Deutsch, C.and McWilliams, B. Baschek, P. P. Sullivan, and D. Chiba. Parameterizing bubble-mediated air-sea gas exchange and its effect on ocean ventilation. *Global Biogeochemical Cycles*, 27(3):894–905, 2013. ISSN 08866236. doi: 10.1002/gbc.20080. URL `http://onlinelibrary.wiley.com/doi/10.1002/gbc.20080/full`.

[39] C. Stolle, K. Nagel, M. Labrenz, and K. JâĹŽÂžrgens. Succession of the sea-surface microlayer in the coastal baltic sea under natural and experimentally induced low-wind conditions. *Biogeosciences*, 7(9):2975–2988, 2010. ISSN 1726-4189. doi: 10.5194/bg-7-2975-2010.

[40] J. Weitz, C. Stock, S. Wilhelm, L. Bourouiba, L. Coleman, A. Buchan, M. Follows, J. Fuhrman, L. Jover, J. Lennon, M. Middelboe, D. Sonderegger, C. Suttle, J. Taylor, W. Thingstad, T. andWilson, and K. Wommack. A multitrophic model to quantify the effects of marine viruses on microbial food webs and ecosystem

processes. *International Society of Microbial Ecology Journal*, 9:1352âĂŞ1364, 2015.

[41] J-H Liang, J. C. McWilliams, and N. Gruber. High-frequency response of the ocean to mountain gap winds in the northeastern tropical pacific. *Journal of Geophysical Research*, 114(C12), 2009. ISSN 0148-0227. doi: 10.1029/2009jc005370. URL `http://onlinelibrary.wiley.com/doi/10.1029/2009JC005370/full`.

[42] G.T. Wallace Jr. and R.A. Duce. Transport of particulate organic matter by bubbles in marine waters. *Limnology and Oceanography*, 23(6):1155âĂŽÃĎÃň1167, 1978. URL `http://onlinelibrary.wiley.com/doi/10.4319/lo.1978.23.6.1155/full`.

[43] H. Lhuissier and E. Villermaux. Bursting bubble aerosols. *J. Fluid Mech.*, 696: 5–44, 2012.

[44] T. P. Liyana-Arachchi, Z. Zhang, F. S. Ehrenhauser, P. Avij, K. T. Valsaraj, and F. R. Hung. Bubble bursting as an aerosol generation mechanism during an oil spill in the deep-sea environment: molecular dynamics simulations of oil alkanes and dispersants in atmospheric air/salt water interfaces. *Environ Sci Process Impacts*, 16(1):53–64, 2014. ISSN 2050-7895-2050-7887. doi: 10.1039/c3em00391d. URL `https://www.ncbi.nlm.nih.gov/pubmed/24296764`.

[45] A. H. Woodcock, C. F. Kientzler, A. B. Arons, and D. C. Blanchard. Giant condensation nuclei from bursting bubbles. *Nature*, 172:1144–1145, 1953.

[46] E. R. Baylor, V. Peters, and M. B. Baylor. Water-to-air transfer of virus. *Science*, 197(4305):763–4, 1977. ISSN 0036-8075.

[47] Duncan C. Blanchard, Lawrence D. Syzdek, and Martin E. Weber. Bubble scavenging of bacteria in freshwater quickly produces bacterial enrichment in airborne jet drops. *Limnology and Oceanography*, 26(5):961–964, 1981. ISSN 1939-5590. doi: 10.4319/lo.1981.26.5.0961.

[48] D. Yu Baturenko, Yu M. Chernoberezhskii, A. V. Lorentsson, and A. N. Zhukov. Effect of pH on the Aggregation Stability of Microcrystalline Cellulose Dispersions in Aqueous 0.1 M NaCl Solutions. *Colloid Journal of the Russian Academy of Sciences: Kolloidnyi Zhurnal*, 65(6):666–671, 2003. ISSN 1061933X. doi: 10.1023/B:COLL.0000009107.51130.a6.

[49] Duncan C Blanchard. *Air-Sea Exchange of Gases and Particles*, chapter The Production, Distribution, and Bacterial Enrichment of the Sea-Salt Aerosol, pages 407–454. Springer Netherlands, Dordrecht, 1983. ISBN 978-94-009-7169-1. doi: 10.1007/978-94-009-7169-1_7.

[50] Y. Toba. Drop production by bursting of air bubbles on the sea surface (II) Theoretical study on the shape of floating bubbles. *J. Oceanogr. Soc. Japan*, 15 (3):121–130, 1959.

[51] H.M. Princen. Shape of a fluid drop at a liquid-liquid interface. *J. Coll. Sci. Imp. U. Tok.*, 18:178–195, 1963. ISSN 00958522. doi: 10.1016/0095-8522(63)90008-4.

[52] G. B. Deane and M. D. Stokes. Scale dependence of bubble creation mechanisms in breaking waves. *Nature*, 418:839–844, 2002. ISSN 0028-0836. doi: 10.1038/nature00967.

[53] E. R. Lewis and S. E. Schwartz. *Sea salt aerosol production: mechanisms, methods, measurements, and models–A critical review*, volume 152. American geophysical union, 2004.

[54] G. de Leeuw, E. L. Andreas, M. D. Anguelova, C. W. Fairall, E. R. Lewis, C. O'Dowd, M. Schulz, and S. E. Schwartz. Production flux of sea spray aerosol. *Rev. Geophys.*, 49(2), 2011. ISSN 1944-9208. doi: 10.1029/2010RG000349.

[55] Wang, X. *et al.* The role of jet and film drops in controlling the mixing state of submicron sea spray aerosol particles. *Proc. Natl. Acad. Sci. U.S.A.*, 114: 6978–6983, 2017. doi: 10.1073/pnas.1702420114. URL `http://www.pnas.org/content/early/2017/06/14/1702420114.abstract`.

[56] H. Lhuissier and E. Villermaux. Bursting bubble aerosols. *J. Fluid Mech.*, 696: 5–44, 2012. ISSN 0022-1120. doi: 10.1017/jfm.2011.418. URL `http://www.journals.cambridge.org/abstract\_S0022112011004186`.

[57] L. Bourouiba and J. WM Bush. Drops and bubbles in the environment. In *Handbook of Environmental Fluid Dynamics, Volume One: Overview and Fundamentals*, pages 427–439. CRC Press, 2012.

[58] J. Wu. Evidence of sea spray produced by bursting bubbles. *Science*, 212(4492): 324–326, 1981. ISSN 0036-8075.

[59] H. Leclerc, L. Schwartzbrod, and E. Dei-Cas. Microbial agents associated with waterborne diseases. *Crit. Rev. Microbiol.*, 28(4):371–409, 2002.

[60] O. Stuhlman Jr. The mechanics of effervescence. *Physics*, 2(6):457–466, 1932.

[61] A. H. Woodcock. Note concernin 9 human respiratory irritation associated with high concentrations of plankton and mass mortality of marine organisms. *J. Marine Res.*, 7:56–62, 1948.

[62] A. H. Woodcock. Bursting bubbles and air pollution. *Sewage Ind. Waste*, 27 (10):1189–1192, 1955.

[63] E. S. Harold. Ejection of microalgae into the air via bursting bubbles. *J. Allergy Clin. Immunol.*, 53(3):185 – 188, 1974. ISSN 0091-6749.

[64] F. B. Higgins. *Bacterial aerosols from bursting bubbles.* PhD thesis, Georgia Institute of Technology, 1964.

[65] D. C. Blanchard. Jet drop enrichment of bacteria, virus, and dissolved organic material. *Pure Appl. Geophys.*, 116(2):302–308, Mar 1978. ISSN 1420-9136.

[66] A. Carducci, E. Tozzi, E. Rubulotta, B. Casini, L. Cantiani, E. Rovini, M. Muscillo, and R. Pacini. Assessing airborne biological hazard from urban wastewater treatment. *Water Research*, 34(4):1173 – 1178, 2000. ISSN 0043-1354.

[67] S. Laitinen, J. Kangas, M. Kotimaa, and J. Liesivuori. Workers' exposure to airborne bacteria and endotoxins at industrial wastewater treatment plants. *Am. Ind. Hyg. Assoc. J.*, 55(11):1055, 1994.

[68] R. L. Ferguson and A. V. Palumbo. Distribution of suspended bacteria in neritic waters south of long island during stratified conditions1. *Limnology and Oceanography*, 24(4):697–705, 1979. ISSN 1939-5590.

[69] D. C. Blanchard. The electrification of the atmosphere by particles from bubbles in the sea. *Prog. Oceanogr.*, 1(Supplement C):73 – 202, 1963. ISSN 0079-6611.

[70] M. E. Weber. Collision efficiencies for small particles with a spherical collector at intermediate reynolds numbers. *J. Separation Process Technol.*, pages 29–33, 1981.

[71] P. A. Baron and K. Willeke. Respirable droplets from whirlpools: Measurements of size distribution and estimation of disease potential. *Environ. Res.*, 39(1):8 – 18, 1986. ISSN 0013-9351.

[72] D. E. Spiel. On the births of film drops from bubbles bursting on seawater surfaces. *J. Geophys. Res. Oceans*, 103(C11):24907–24918, 1998. ISSN 2156-2202.

[73] F. Resch and G. Afeti. Film drop distributions from bubbles bursting in seawater. *J. Geophys. Res. Oceans*, 96(C6):10681–10688, 1991. ISSN 2156-2202.

[74] CDC. Multistate outbreak of shiga toxin-producing escherichia coli o157:h7 infections linked to i.m. healthy brand soynut butter (final update). 2017.

[75] D. L. Gally and M. P. Stevens. Microbe profile: Escherichia coli O157:H7 âĂŞ notorious relative of the microbiologistworkhorse. *Microbiology*, 163(1):1–3, 2017.

[76] U.S. Department of Health and Human Services. *Biosafety in Microbiological and Biomedical Laboratories, 5th ed.* 2016. URL `https://www.cdc.gov/biosafety/publications/bmbl5/BMBL.pdf`.

[77] J. G. Sutcliffe. Nucleotide sequence of the ampicillin resistance gene of Escherichia coli plasmid pBR322. *PNAS*, 75(8):3737–3741, 1978.

[78] K. Lawrence and M. Anthony. The effects of ampicillin on the growth of escherichia coli. 2013.

[79] S. Sutton. Measurement of cell concentration in suspension by optical density. 2017. URL `http://www.microbiol.org/resources/monographswhite-papers/measurement-of-cell-concentration-in-suspension-by-optical-density/`.

[80] PG. de Gennes, F. Brochard-Wyart, and Quere D. *Capillarity and Wetting Phenomena: Drops, Bubbles, Pearls, Waves.* Cambridge: Harvard University Press, 2004.

[81] G. S. Settles. *Schlieren and Shadowgraph Techniques: Visualizing Phenomena in Transparent Media.* Experimental Fluid Mechanics. ISBN 9783642566400.

[82] The dynamics of thin sheets of fluid. iii. disintegration of fluid sheets. *Proc. Math. Phys. Eng. Sci.*, 253(1274):313–321, 1959. ISSN 0080-4630. doi: 10.1098/rspa.1959.0196.

[83] F. E. C. Culick. Comments on a ruptured soap film. *J. Appl. Phys.*, 31(6): 1128–1129, 1960. doi: 10.1063/1.1735765.

[84] A. Korpel, D. Mehrl, and H. H. Lin. Schlieren imaging of sound fields. In *IEEE 1987 Ultrasonics Symposium*, pages 515–518. IEEE, 1987.

[85] Y. D. Afanasyev, G. T. Andrews, and C. G. Deacon. Measuring soap bubble thickness with color matching. *Am. J. Phys.*, 79(10):1079–1082, 2011.